

CRUISE REPORT
SERIAL # 90018 FARNELLA JUL 19 - AUG 3 1990
+ # 90027 NO DATA IN LIBRARY
CHIEF SCIENTIST KARL/DRAKE

Rec'd 1/31/91
In Adm. Cuseo

DEPARTMENT OF THE INTERIOR

U.S. GEOLOGICAL SURVEY

Progress Report on Status of Analysis and Interpretation of Data

Collected on Cruises F7-90-NC and F8-90-NC

Farallon Escarpment, 19 July to 3 August and 5 to 17 August, 1990

by

H.A. Karl, D.E. Drake, W.C. Schwab, B.D. Edwards, H.J. Lee, and J.L. Chin

November 1, 1990

This report is preliminary and has not been reviewed for conformity U.S. Geological Survey editorial standards. Any use of trade names descriptive purpose only and does not imply endorsement by the USGS.

INTRODUCTION

This report is the first of two interim reports to be submitted prior to the final report (due August 1991) that describe the progress of the analysis of data collected on the Farallon Escarpment on cruises F7-90-NC and F8-90-NC during 19 July to 3 August and 5 to 17 August, 1990. In this report we describe (1) the sidescan sonar mosaic, (2) examples of the high-resolution seismic-reflection profiles, (3) the surficial grain-size data, and (4) some of the physical properties of the sediment as determined by geotechnical analyses. The interpretations based on these data are preliminary and will, undoubtedly, be modified in the final report. Therefore, no conclusions should be drawn from the data presented herein beyond those specifically stated by the authors in this report.

SIDESCAN SONAR MOSAIC

Appendix I is a preliminary geomorphic and geologic interpretation of the SeaMARC sidescan sonar mosaic that was provided to the U.S. Environmental Protection Agency upon completion of cruise F7-90-NC and F8-90-NC. The interpretive overlay is at a scale of 1:100,000. The sidescan sonar mosaic is an acoustic image of the seafloor in that acoustic energy transmitted from the sidescan tow vehicle is reflected and backscattered from the seafloor. These acoustic data have been computer processed so that the mosaic represents a true plan view of the seafloor such that features on the seafloor seen on the mosaic are in their correct spatial position (note the discussion of navigation below) and their true geometric shape. The shades of gray ranging from black to white that define the features of the seafloor on the mosaic represent varying energy levels of acoustic backscatter. The darker shades correspond to higher backscatter levels. Many complex factors determine how

sound is backscattered and reflected from the seafloor. Furthermore, the sonar instrument used for this survey, SeaMARC IA, is a deep-towed 30 kHz system. Sound transmitted at this mid-range frequency (high frequency being 100 kHz and low frequency being about 6.5 kHz) is capable of penetrating below the surface of the seabed under certain conditions. Therefore, some of the features seen on the mosaic may not represent features on the seafloor, but rather features buried at an unknown depth beneath the surface. Consequently, the interpretation of the acoustic mosaic is not as straightforward as viewing and interpreting an aerial photograph or satellite image which show only surficial features. Interpretation of sonograph images is an art as well as a science. Other data sets should be used to supplement and complement the sonar data so that the sonar images can be interpreted as accurately as possible. By so doing, the sonar image can be verified or "ground-truthed". For that reason (as well as other geologic reasons) we collected high-resolution seismic-reflection data and sediment cores in the survey area.

The first aspect to note on the mosaic is the basic difference in shading or tone between the northern and southern halvess which correlate with a difference in the ruggedness (topography) of the seafloor. The northern half of the study area is very rugged with numerous submarine canyons and ridges (figs. 1 and 2). Many (but not all) of these have been delineated on the interpretive overlay. Sediment in this northern province, as determined from the mosaic and the high-resolution seismic-reflection profiles, appears to be sparsely distributed and of variable thickness. The southern province is much less rugged overall (fig. 3). Sediment appears more uniformly distributed, but still of variable thickness. Prominent geomorphic features in the southern province include Pioneer Canyon (fig. 4) and Pioneer Seamount (fig. 5). Pioneer Seamount is volcanic basement (dark areas on mosaic) that is covered by hemipelagic sediment (light areas). The expansive light gray to white areas north and south of Pioneer Canyon are gently sloping, relatively flat and featureless plains of

mud (figs. 3 and 4).

We expected to find abundant evidence of mass movement of sediment (submarine landslides) when we embarked on the cruise, however, we observed relatively few on the mosaic in the study area. Several areas of possible slumps have been identified on the interpretive overlay. These are on steep slopes and on the walls of submarine canyons. There is no unequivocal evidence of mass wasting on the expansive plains north and south of Pioneer Canyon. Computer enhancements of the sonar imagery which we are working on may reveal some areas of mass wasting. However, the sparsity of mass wasting is corroborated by the seismic-reflection profiles and visual inspection of sediment cores. Preliminary geotechnical analysis of the cores indicate that these slopes are marginally stable under seismic loading conditions (see section entitled Geotechnical Assessment). The lack of large slumps and slides is surprising on a section of continental margin that is subjected to numerous large earthquakes.

NAVIGATION

Four systems were used to navigate the ship: (1) Global Positioning System (GPS); (2) LORAN-C, either hyperbolic or rho-rho; (3) shore-based transponder net (Del Norte system); and (4) a long baseline bottom transponder net. The primary system used for real-time positioning was chosen either manually by the navigator or automatically by the shipboard computer. Steering of the ship was aided by a trackline-following program displayed on a CRT screen both at the helm and at the navigator's station. Positional accuracy of navigation tracks typically varied between 50 and 100 m of the postplotted tracks (appendices II-VI are postplotted tracklines and station locations). The long baseline transponder net was emplaced in the central part of the study area on the submarine plain to

the north of Pioneer Canyon. The position of each of the six transponders in the net was accurately determined using the best of the three navigation systems described above. The long baseline net was used to accurately fix the location of the center of the sonar mosaic. Positional uncertainty increases with increasing distance from the center of the net. When the ship was within the range of the net, the bottom transponders were used for navigation. One of the three other systems was used for navigation when outside of the net. The black rectangular areas in the center of the mosaic are zones of no data. These areas represent a spatial jump which is the magnitude of the positional error between navigation within the net and outside of the net.

The navigation coordinates entered into the SeaMARC data acquisition/processing computers were those of the ship's position and not the position of the tow vehicle. The position of the tow vehicle relative to the ship was a function of the length of cable deployed and the speed of the ship. Since we could not range acoustically on the tow vehicle owing to acoustic interference, it was necessary to estimate the position of the tow vehicle with respect to the ship. This difference between ship and tow vehicle position is called "layback".

The sidescan mosaic described and interpreted in this report was constructed onboard ship by matching features on adjacent sonographs and progressively constructing a mosaic of the seafloor. The sidescan system was set at a 5-km swath width and tracklines spaced 4 km apart giving about 20% overlap between adjacent swaths. Features in the central and southern part of the mosaic are accurately located on the seafloor with respect to latitude and longitude. Features in the extreme northern part of the mosaic are offset by as much as 2 km to the northwest from their true position on the seafloor. The final mosaic will be corrected for these navigational errors.

HIGH RESOLUTION SEISMIC REFLECTION PROFILES

High resolution seismic reflection profiles used in this interim report were acquired using a 3.5 kHz subbottom profiler system. This system is a precision depth recorder that utilizes a towfish, graphical recorder, and various power, filtering, and annotating instruments to produce the seismic reflection profiles illustrated . The towfish is towed along side the vessel and collects continuous data which is then filtered and displayed on an analog record. The towfish emits a high frequency (3.5 kHz) sound pulse which is reflected off of the seafloor as well as from interfaces within the seabed. Penetration within the seabed varies greatly as a function of several factors. As the seismic reflection profiles show, penetration ranged from 0 to 45 m. The sound pulse emitted is a wide beam in addition to being high in frequency. Thus, it is common on seismic reflection profiles to see features that in reality are not directly beneath the vessel but are to the side(s). These commonly show up on the profiles as side-echoes or hyperbolae. These features are artifacts on the records and not real structures on the seafloor, although side-echos and hyperbolae provide information useful to the overall interpretation.

The seismic reflection profiles illustrated were recorded at a sweep rate of 1-second (travel time from the sound source to the seafloor and back to the sound source) such that, assuming a sound velocity through sea water of 1500 m/second, the full width of the profile displays 750 m in the vertical dimension. The horizontal distance on the profiles varies as a function of paper speed and the speed of the vessel. The paper speed is constant for all profiles such that variation in the horizontal dimension varies chiefly as a function of the ship's speed. Since the ship often averaged over 7 to 8 knots during the collection of these profiles, it is not unreasonable that the exaggeration in the vertical dimension may be 20 times or greater. Hence the profiles often depict a greatly exaggerated view of the seafloor in these profiles.

Features on the seismic reflection profiles can be located geographically by using the position of the vessel on post-plotted navigation as the position of the 3.5 kHz tow fish coincides with that of the vessel at all times. The 3.5 kHz profiles yield a variety of useful information about the external morphology and composition of the seafloor and the internal morphology and acoustic character of the seabed. Interpretations regarding the relief of the seafloor, whether the seafloor represents an erosional or depositional regime, whether sediment failure (mass movement) has occurred, the acoustic nature and stratigraphy of the seabed can all be derived from analysis of the 3.5 kHz profiles. Moreover, this information can be correlated to results derived from side-scan sonar, bathymetry(10 kHz), sampling, and other shipboard collected data. Figure 6 depicts the 3.5 kHz high resolution seismic reflection tracklines referred to below.

Line-22 (Figs. 7a and 7b) is a trackline that traverses the study area from south to north. The southernmost part of the profile (parts "A" and "B") occurs adjacent to the headward portion of Pioneer Canyon. The profile shows that the relatively flat to gently sloping areas that border the heads of Pioneer Canyon are covered by up to 25-30 m of "unconsolidated" sediment. The flanks of the canyon heads however have a typically thin to absent sediment drape. Proceeding north on this line (part "C") it is evident that the topography and sediment thickness change significantly. This change on the 3.5 kHz profiles is coincident with a change on the side scan sonar mosaic that signifies a transition from flat or gently sloping plains (southern province) to highly variable ridge and valley/canyon topography (northern province). Sediment thickness is highly variable and ranges from 0 to 25 m. Note also that on part "C" of line-22 there are several possible sediment failures on relatively steep slopes that border canyons. Preliminary analysis of 3.5 kHz profiles though suggest that most sediment failures occur only on relatively steep slopes that border canyons or bedrock outcrops. The flat to gently sloping plains appear to have few if any sediment failures.

Lines 57 and 60 (Figs. 8 and 9) traverse the flat gently sloping plain that occurs north of Pioneer Canyon from northeast to southwest. These profiles reveal that "unconsolidated" sediment thickness varies from 0 to about 10-15 m and is not continuous from upslope to downslope areas. Both profiles show possible sediment failures towards the downslope part of each profile where the slope of the seafloor increases.

Lines 81 and 82 (Fig. 10) traverse the flat gently sloping plain site that occurs south of Pioneer Canyon. These profiles reveal a discontinuous "unconsolidated" sediment cover that varies from 0 to about 25 m. Both profiles suggest that sediment failure may be present where topography is steep.

SURFICIAL SEDIMENT TEXTURAL CHARACTERISTICS

Thirty-three gravity cores were collected at 23 stations on the continental slope in water depths that ranged from 300 to 3000 m (Fig. 11). Cores varied in length from about 1 m to just under 3 m. Samples for grain-size analyses were collected at the surface and at 1-m intervals down the core (Appendix VII). Maps of mean grain-size and sediment texture for surficial sediment are shown in Figures 12, 13, and 14. Many of the surface samples contain higher percentages of sand than we expected to find in continental slope sediment; slopes are characterized by silts and clays. We do not fully understand the reason for the higher percentage of sand. Usually sandy sediments indicate strong currents or an abundant supply of coarse material. Strong currents are required to transport large amounts of sand from the shelf to the slope; we do not know the current regime on the adjacent shelf. Coarse grained material is present on the continental slope, but usually it is masked or overwhelmed by the fine-grained sediment, and, consequently, the coarse material comprises a small percentage of the total sample. Ordinarily, strong currents on the continental shelf winnow

fine-grained material from shallow water deposits and transport this material in suspension to the lower energy environment of the continental slope where it settles and accumulates on the seabed. The silt and clay continue to accumulate and form thick water-saturated deposits which often become unstable on the steep parts of the continental slope. The sediment deposits on the continental slope in the study area require further investigation.

GEOTECHNICAL ASSESSMENT

Completed Work

We have completed a preliminary analysis of the descriptive physical properties that characterize sediment recovered from the Farallon slope segment. Figure 15 shows the location of the 33 gravity cores collected from 23 stations occupied on the slope. Single gravity cores were collected for stratigraphic and sedimentologic (SS) analyses at 12 of the 23 stations. Two gravity cores were collected at each of the remaining 11 stations, one for stratigraphic/sedimentologic analyses and the other for detailed geotechnical (GT) studies. Stations with GT cores are identified by a star on Figure 15. One occupied station was abandoned without a successful recovery (NR). The coring sites have been grouped into 3 transects that extend from the upper slope down to the base of slope (Fig. 15). For descriptive purposes, depositional environments have been assigned to each station: upper slope ranges from 200 meters to 800 meters, middle slope ranges from 800 meters to 1600 meters, lower slope ranges from 1600 meters to 2000 meters, and the base-of-slope lies below 2000 meters. Table 1 presents detailed station information that pertains to each core.

The stratigraphic/sedimentologic cores (SS) were routinely tested downcore for compressional wave (P-wave) velocity, magnetic susceptibility, natural water content, peak and remolded undrained vane shear strength, and grain size. Figure 16 shows a typical presentation of data collected from each SS core; data for all cores is presented in Appendix

VIII. The P-wave velocity and magnetic susceptibility data were obtained using a newly acquired instrument, the Schultheiss Geotek Multi-Sensor Whole-Core Logger. We have not completed calibration of this prototype instrument and P-wave velocities may vary by more than 2 percent from the values presented in this report. Sediment bulk density was calculated from water content assuming 100% saturation. Sediment vane shear strength was measured using a torque cell attached to a shear vane rotated at a constant 90°/min rate. Both peak (s_{uv}) and remolded (s_r) strengths were obtained using procedures described by Lee (1985). Sensitivity (S_t) was calculated using the relationship:

Grain size was determined by hydrophotometer. Thus far, only P-wave velocity and magnetic susceptibility have been measured on the recovered geotechnical (GT) cores.

Preliminary Stability Analysis

Slope failure occurs when driving stresses exceed the capacity of the sediment to resist the stress (Lee and Edwards, 1986). Three agents commonly produce the downslope driving stress that can trigger slope failure: (1) gravity, (2) ocean waves, and (3) earthquakes. Gravity acts continuously and has a downslope component that increases with the steepness of the slope. Ocean waves produce cyclically varying shear stresses within the sediment column as the wave train passes at the sea surface. As a result of these oscillatory loads, internal pore water pressures can develop which reduce the resistive strength of the sediment. Earthquakes generate cyclically varying stresses within the sediment as well. These stresses vary with earthquake magnitude, distance from the zone of rupture, slope geometry, position within the sediment column, total thickness of the sediment body, and the properties of the effected sediment and underlying rock mass. Earthquake-induced shear stresses also reduce the sediment strength.

The capacity of the sediment to resist driving stresses (i.e., the sediment strength) is a complicated quantity that typically varies with depth in the sediment column, sediment grain characteristics (e.g., grain size, mineralogy, and plasticity), sedimentation history, intensity and rate of loading, type of loading (cyclic or static), duration of loading, and the overall configuration of the slope and regional stratigraphy. For example, the strength developed in sediment in order to resist earthquake shaking is a function of the sediment static and cyclic stress history and sediment physical characteristics. As a consequence of earthquake loading, shear stresses acting on a slope typically are increased while the resistive strength of the sediment typically is reduced due to the generation of excess pore pressures. This condition leads to an increased susceptibility for failure.

The available vane shear and density data allow us to develop a preliminary stability analysis of the slope sediment for both static and seismically loaded conditions; the water depth at these coring sites is too great for wave loading to be a significant factor. Figure 17 shows vane shear measurements for the five cores positioned along Transect B (Fig. 15). A lower bound line that passes through the origin has been drawn for the data set. This line represents a conservative estimate of the peak shear strength throughout the upper part of the sediment column (< 3 meters) in this slope region. Data from cores 3G1, 6G7, and 8G10 lie closest to this line and likely are the most susceptible to failure. Note that these cores extend from the upper to the lower slope environments. Specifically, we will use a value of 5 kPa at a subbottom depth of 2 meters for the preliminary analysis (circle around part of core 3G1 in Fig. 17).

Static Failure Condition. At failure under static (gravitational loading) conditions, gravitational shear stresses will equal or exceed the available resistive shear stress of the sediment. In a simplified analysis, static shear stress can be defined by:

$$\tau = \sigma'_v \sin \alpha \dots \dots \dots \quad (2)$$

in which τ is the shear stress, σ'_v is the effective overburden stress, and α is the slope angle. The effective overburden stress (σ'_v) is the part of the overburden stress that acts across sediment grain contacts and is equal to the buoyant or submerged sediment density times the depth in the sediment column. Evaluating σ'_v for core 3G1, we obtained a value of 11.7 kPa at 2 meters. At failure, the downslope shear stress is equal to the shear strength. Setting $\tau = s_{uv} = 5$ kPa and solving eq. 2 for α yields a conservative estimate that a slope of 25° is required before failure by gravitational loading occurs. The slope in the region of core locations along Transect B is about 3 degrees indicating that failure of the existing sediment under static gravitational loading conditions is unlikely.

Seismically Loaded Condition. As evidenced by the 1906 San Francisco earthquake (local Richter magnitude, $M_L \approx 8.1$ to 8.3) and the more recent October 17, 1989, Loma Prieta earthquake ($M_L = 7.1$), the San Francisco Peninsula clearly is a seismically active area (Benuska, 1990). The trace of the north coast segment of the San Andreas fault lies about 50 km northeast of the study area and is thought to be capable of producing a maximum credible earthquake of about $M_L = 8.25$ (Greensfelder, 1974). Detailed information on soil and rock response to such large seismic events is sparse and predictive equations of peak horizontal accelerations from major earthquakes are constrained only within the magnitude range of 5.0 to 7.7 (Joyner and Fumal, 1985). Thus, inferences regarding soil response to a seismic event in the range of $M_L = 8.25$ should be interpreted with caution. With this caveat, the estimated peak horizontal acceleration that can be expected in the study area in response to a $M_L = 8.25$ event on the San Andreas fault over the next 100 years is about 0.16 g (Thenhaus et al., 1980, plate 2; Joyner and Fumal, 1985, Fig. 88).

On level ground, the average seismically-induced shear stress for peak horizontal seismic

accelerations has been estimated by Seed and Idriss (1971) as:

in which a_{max} is the maximum horizontal earthquake acceleration, and r_d is a stress reduction term that varies with depth. The total overburden stress (σ_v) is equal to the total sediment density times the depth in the sediment column. At shallow subbottom depths (< 3 meters) r_d is approximately equal to 1.0 (Seed and Idriss, 1974, Fig. 4). For a slope environment, Eqns. 2 and 3 can be summed to obtain the total downslope shear stress acting during an earthquake:

Setting the downslope shear stress, τ , equal to the vane shear strength of core 3G1 at 2 meters and solving for a_{max} leads to a value of about 0.2 g; that is, horizontal seismic accelerations on the order of 0.2 g or greater can cause sediment failure. The prediction that the study area has (the 1906 event) or will experience accelerations on the order of 0.16 g suggests that the Transect B slope segment is only marginally stable under seismic loading conditions.

Another way to view the slope stability problem is to compare the geotechnical characteristics along the Transect B slope segment with those of known seismically-induced failures along the west coast of the United States. In previous studies (Lee and Edwards, 1986), we backcalculated a seismic strength factor (k) from measured physical properties and observed slope failures in high seismicity areas of Alaska and California. We found that values of k less than or equal to 0.13 corresponded with locations of observed slope failure. Using a relation for k (a modified version of eq. 5 of Lee and Edwards, 1986) we calculated a value of 0.14 for Transect B. Thus, this empirical approach also suggests that existing sediment in the Transect B slope segment is marginally stable under strong seismic loading.

Summary and Further Analysis. Our preliminary findings, based on vane shear and density data, are that the slope sediment in the area of Transect B is stable under static gravitational loading but is likely to be only marginally stable under the strong seismic loading conditions that are likely to be experienced in response to a major event on the San Andreas fault. This conclusion is preliminary and must be evaluated further by additional and more sophisticated geotechnical testing and analysis. We will examine how the sediment behaves under cyclic loading; that is, will the sediment experience sufficient strength degradation during an earthquake such that a landslide will result? On the assumption that the sampled soil profiles (< 3 meters of recovery) accurately reflect the sediment facies at greater subbottom depth, we will extend our analysis throughout the entire unconsolidated soil profile. We are presently designing a static and cyclic triaxial testing program that will answer these questions and that will allow us to constrain and refine our initial interpretations based on vane shear and density data. We will then apply these findings to a regional interpretation of slope stability throughout the study area.

Our finding that the existing slope sediment is marginally stable under seismic loading conditions is somewhat surprising given the lack of evidence for sediment failure in either the side-scan sonar data or the seismic-reflection data. Our preliminary analysis only evaluates when initial failure occurs due to seismic loading, and this condition of shear stress exceeding shear strength may only occur for a brief period of time. The resulting failure may not look like a landslide and may only involve limited downslope translation along thinly - seated shear planes. Also, the thinness of the unconsolidated soil profile (zero to about 45 meters thick) may preclude the development of large, readily identifiable failure masses in some slope areas.

* Further, our analyses are preliminary attempts to evaluate the stability of existing slope

sediment. We do not have sufficient data to address the important questions of (1) how the slope sediment will behave in response to rapid loading by deposition of dredge spoils or (2) how stable the dredge spoil pile will be once deposited on top of these sediments. These are important questions that should be considered in evaluating the Farallon slope study area as a potential dredge spoil site.

ACKNOWLEDGEMENTS

Norman Maher did the grain-size analyses, constructed many of the computer graphics, and drafted many of the figures for this report and Willie McArthur performed water content and sediment bulk density analysis. We are very appreciative of their skills and efforts. William Danforth and Tom O'Brien led the team that processed the SeaMARC 1A data and produced the sonographic images for the seafloor mosaic. Their efforts enabled us to construct a computer processed sidescan sonar mosaic onboard ship. Jesus Baraza assisted with shipboard whole-core logger and vane-shear strength measurements. We thank the officers and crew of the R/V Farnella and the scientific watchstanders and navigators who enabled us to collect quality data at sea.

Nomenclature

GT = core collected for geotechnical analyses

SS = core collected for stratigraphic/sedimentologic analyses

S_t = sensitivity

a_{max} = maximum horizontal earthquake acceleration

k = a backcalculated seismic strength factor (from Lee and Edwards, 1986)

r_d = stress reduction term (approximately = 1 for shallow subbottom depths)

s_r = remolded vane shear strength

s_{uv} = peak undrained vane shear strength

α = angle of slope (in degrees)

σ_v = total overburden stress

σ'_v = effective overburden stress

τ = shear stress

References

- Benuska, Lee, ed., 1990, Loma Prieta Earthquake Reconnaissance Report, Earthquake Spectra, The Professional Journal of Earthquake Engineering Research Institute, supplement to v. 6, 448 p.
- Greensfelder, R.W., 1974, Maximum credible rock acceleration from earthquakes in California: California Division of Mines and Geology, Map Sheet 23.
- Joyner, W.B. and Fumal, T.E., 1985, Predictive mapping of earthquake ground motion: *in* Ziony, J.I., ed., Evaluating Earthquake Hazards in the Los Angeles Region - An Earth-Science Perspective: U.S. Geological Survey Professional Paper 1360, p. 203-220.
- Lee, H.J., 1985, State of the art: Laboratory determination of the strength of marine soils: *in* Chaney, R.C. and Demars, K.R., Strength Testing of Marine Sediments: Laboratory and In-Situ Measurements, American Society for Testing and Materials, STP 883, p. 181-250.
- Lee, H.J., and Edwards, B.D., 1986, Regional method to assess offshore slope stability: Jour. Geotechnical Engineering, American Society of Civil Engineers, v. 112, p. 489-509.
- Seed, H.B., and Idriss, I.M., 1971, Simplified procedure for evaluating soil liquefaction potential: Jour. Soil Mechanics and Foundation Division, American Society of Civil Engineers, v. 97, no. SM9, p. 1249-1273.
- Thenhaus, P.C., Perkins, D.M., Ziony, J.I., and Algermissen, S.T., 1980, Probabilistic estimates of maximum seismic horizontal ground motion on rock in coastal California and the adjacent outer continental shelf: U.S. Geological Survey Open-File Report 80-924, 69 p.

LIST OF FIGURES

- Figure 1. Example of sidescan mosaic showing rugged canyon and ridge topography that characterizes the northern part of the study area.
- Figure 2. Another example of the sidescan mosaic that illustrates the rugged canyon and ridge topography that characterizes the northern part of the study area.
- Figure 3. Part of sidescan sonar mosaic illustrating expansive "plains" of sediment that typify the southern part of the study area.
- Figure 4. Central part of Pioneer Canyon as revealed by SeaMARC system. Note the flat floor and numerous gullies on the canyon walls.
- Figure 5. Pioneer Seamount as revealed on sonar mosaic.
- Figure 6. Location of high-resolution seismic-reflection profiles discussed in text.
- Figure 7a. High-resolution seismic-reflection profile 22, parts A and B.
- Figure 7b. High-resolution seismic-reflection profile 22, parts C and D.
- Figure 8. High-resolution seismic-reflection profile 57.
- Figure 9. High-resolution seismic-reflection profile 60.
- Figure 10. High-resolution seismic-reflection profiles 81 and 82.
- Figure 11. Location of gravity core stations.
- Figure 12. Mean grain-size of surficial sediment samples.
- Figure 13. Surface sediment texture.
- Figure 14. Pie diagrams illustrating percentages of sand, silt, and clay in surface sediment.
- Figure 15. Index map showing location of stratigraphic/sedimentologic (SS) and geotechnical (GT) cores. Cores have been grouped into three transects that extend from the upper slope to the base-of-slope environments.
- Figure 16. Plot illustrating the typical presentation of descriptive physical property data from gravity cores collected across the Farallon slope. See Appendix VIII for the complete data set.
- Figure 17. Plot of peak undrained vane shear strength versus depth for all stratigraphic/sedimentologic (SS) cores collected along Transect B. The bold line passing through the origin represents a lower bound for the strength data. This line was used to establish a conservative estimate for soil strength in the preliminary slope stability analysis.
- Table 1. Listing of core characteristics for each of the 24 occupied stations.

LIST OF APPENDICES

- Appendix I. Interpretative overlay of sidescan sonar mosaic.
- Appendix II. Sidescan sonar tracklines.
- Appendix III. High-resolution seismic-reflection (3.5 kHz) tracks cruise F7-90-NC.
- Appendix IV. High-resolution seismic-reflection (3.5 kHz) tracks cruise F8-90-NC.
- Appendix V. Gravity core station locations cruise F8-90-NC.
- Appendix VI. Camera station transects cruise F8-90-NC.
- Appendix VII. Grain-size analyses cruise F8-90-NC.
- Appendix VIII. Plots of downcore variation in descriptive physical properties for gravity cores collected during cruise F8-90-NC.

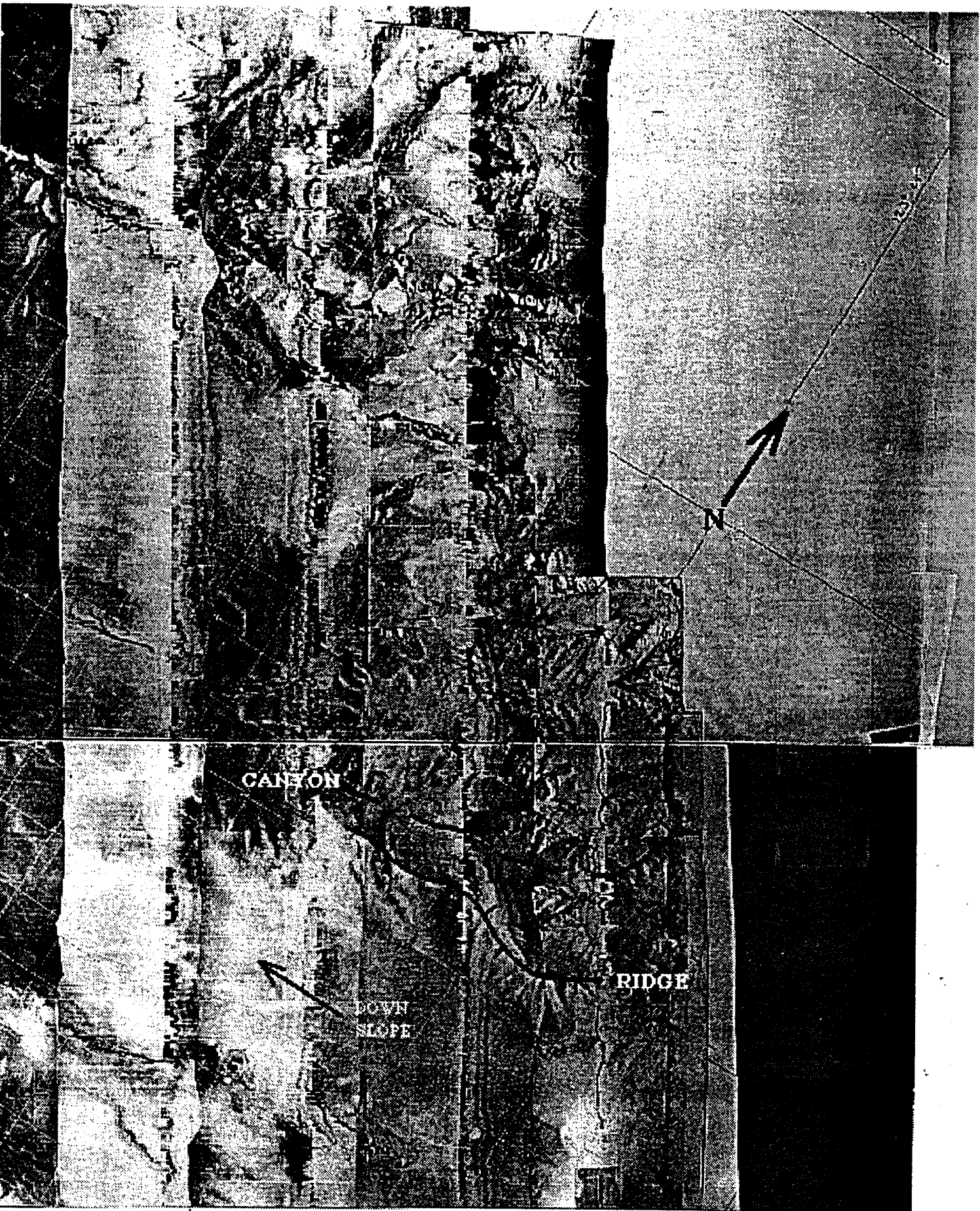


Figure 1

RIDGE AND

CANYON

TOPOGRAPHY

Figure 2

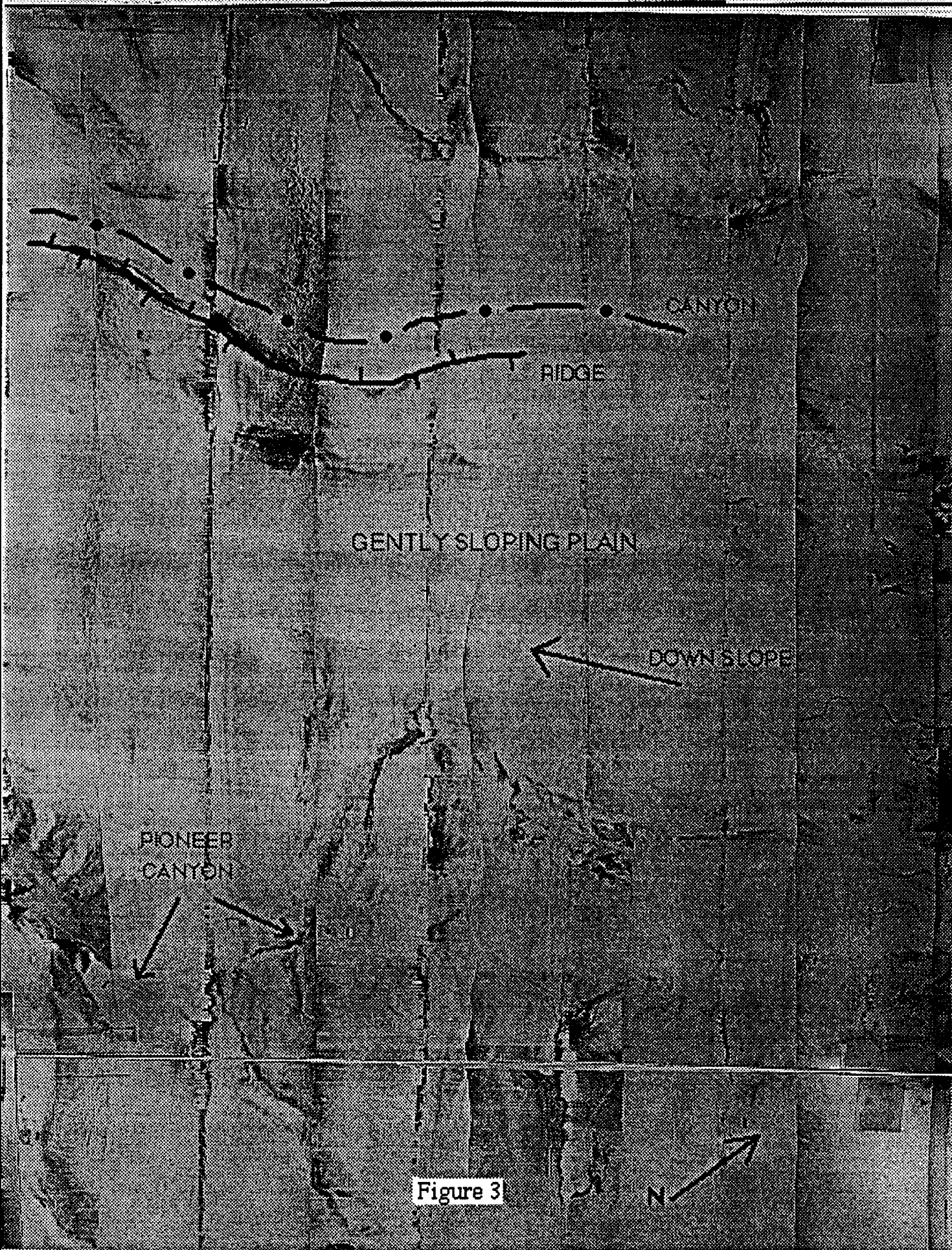




FIGURE 4



FIGURE 5

Figure 6

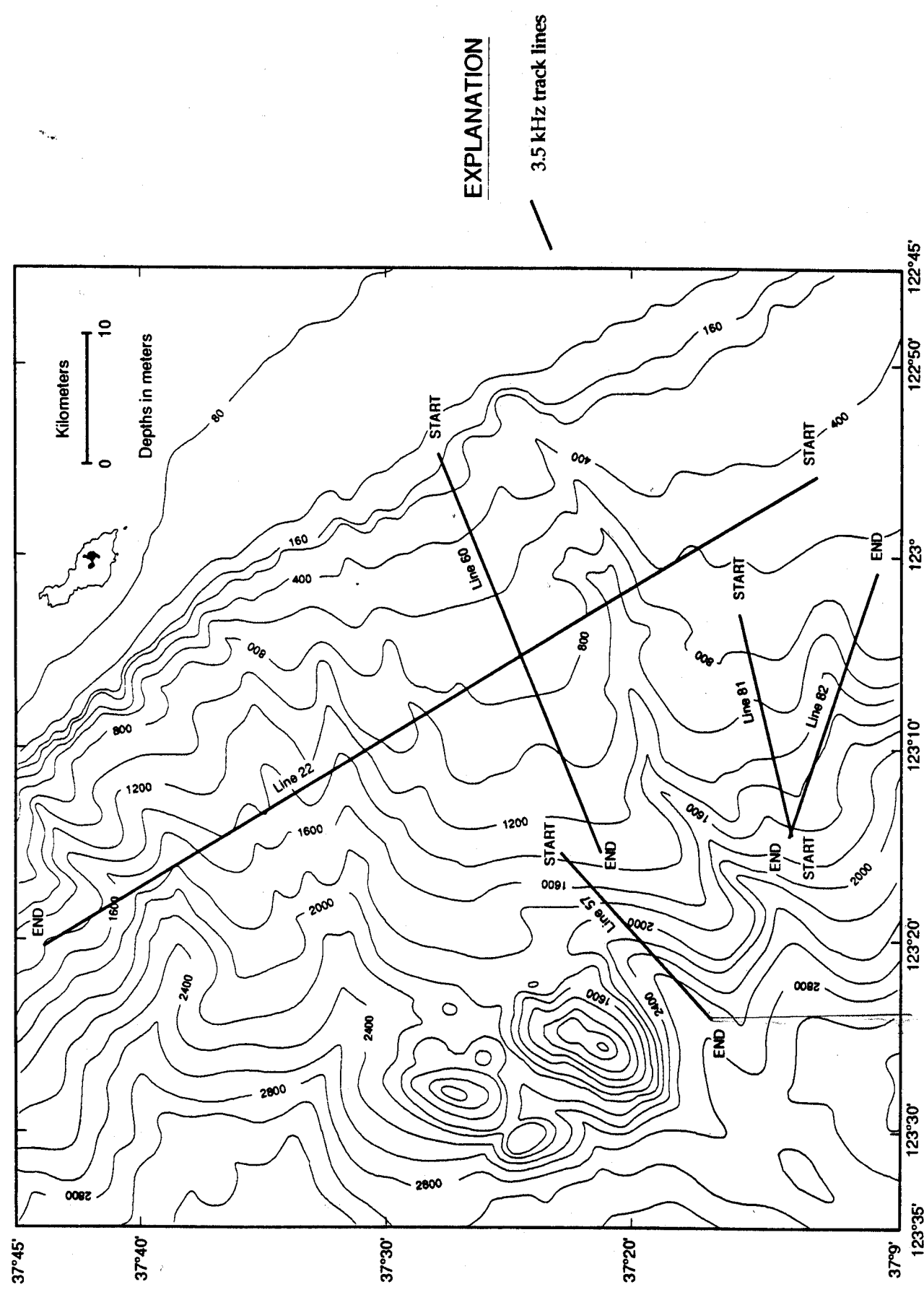


Figure 7a

Line 22

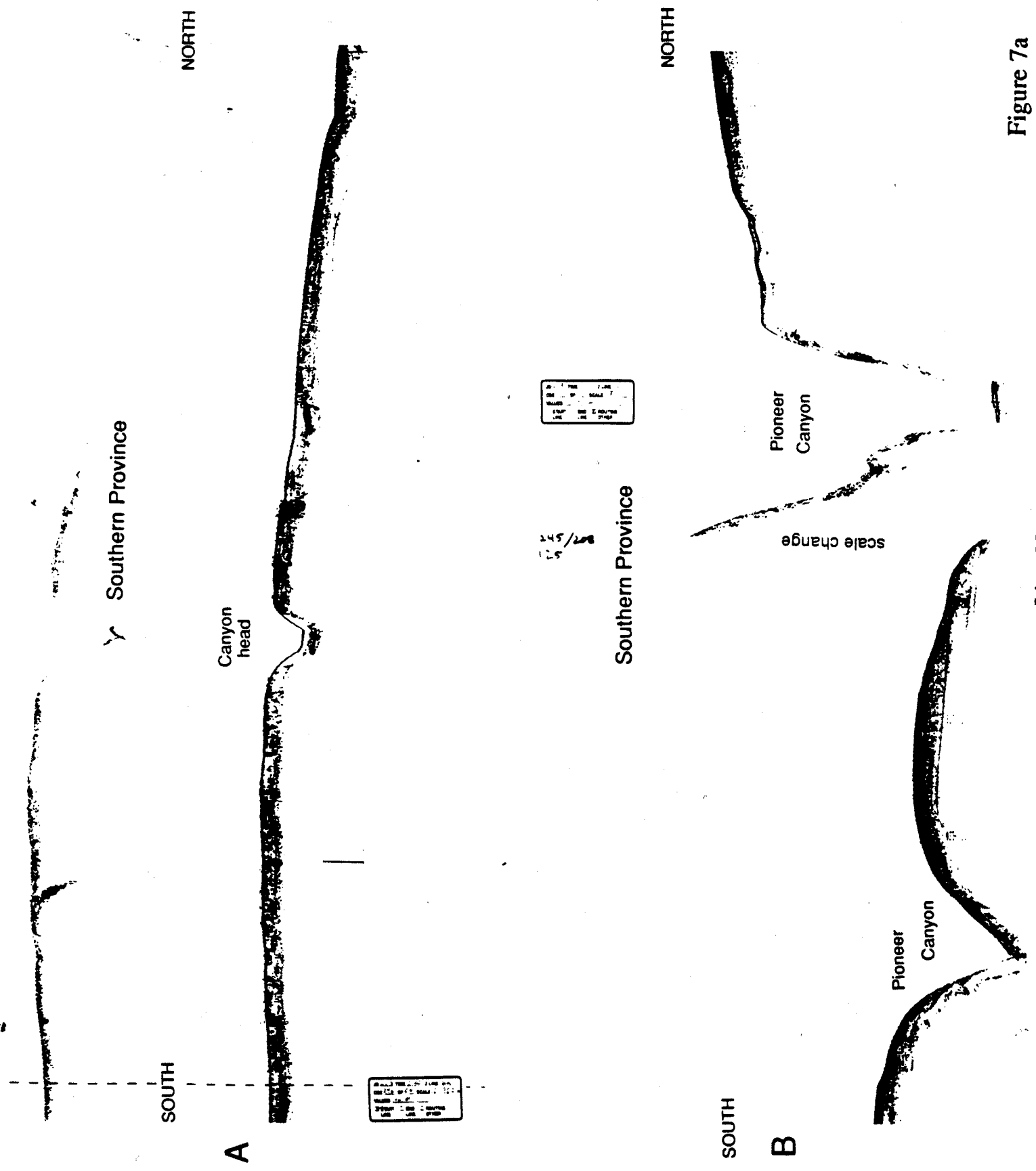
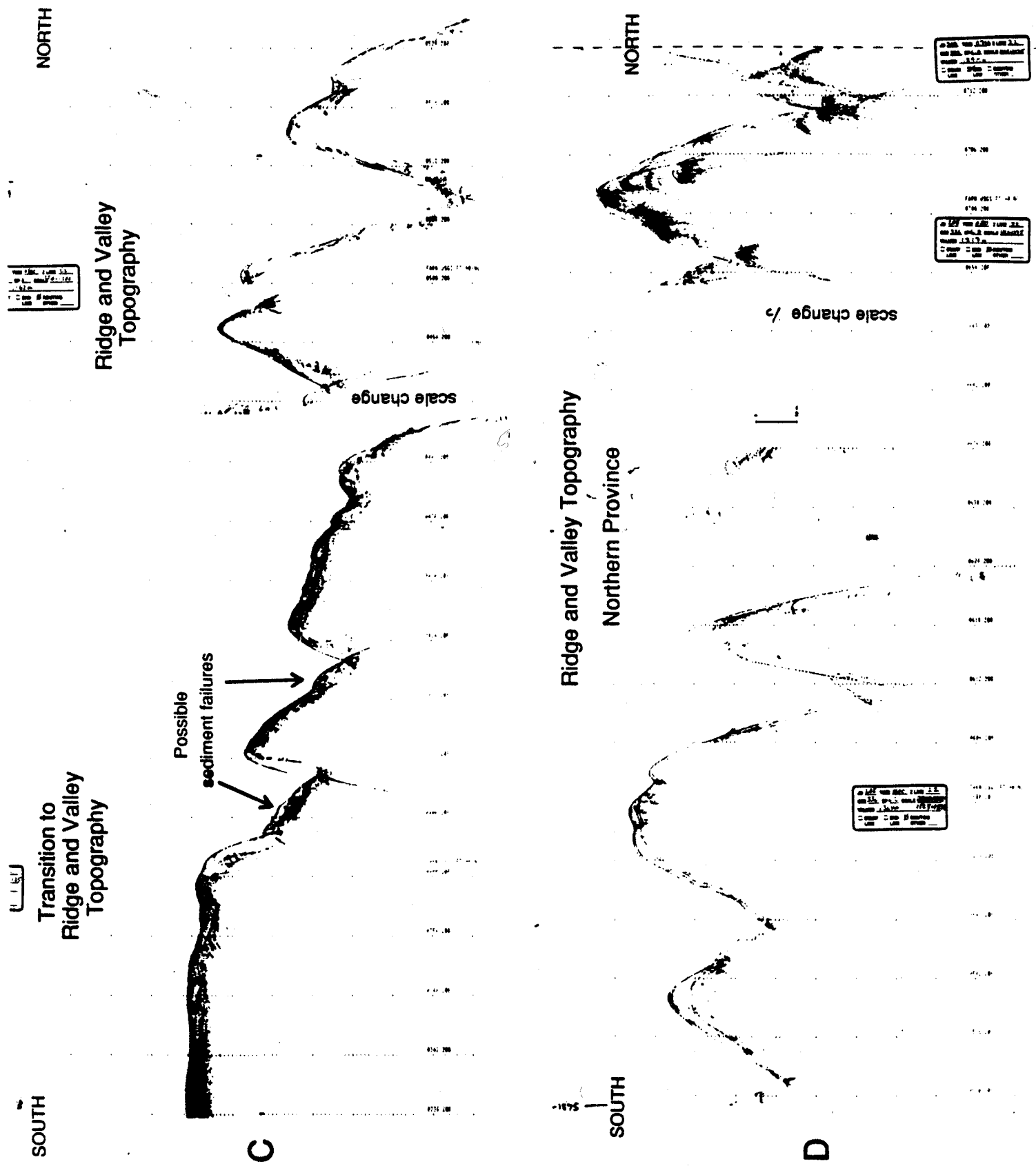
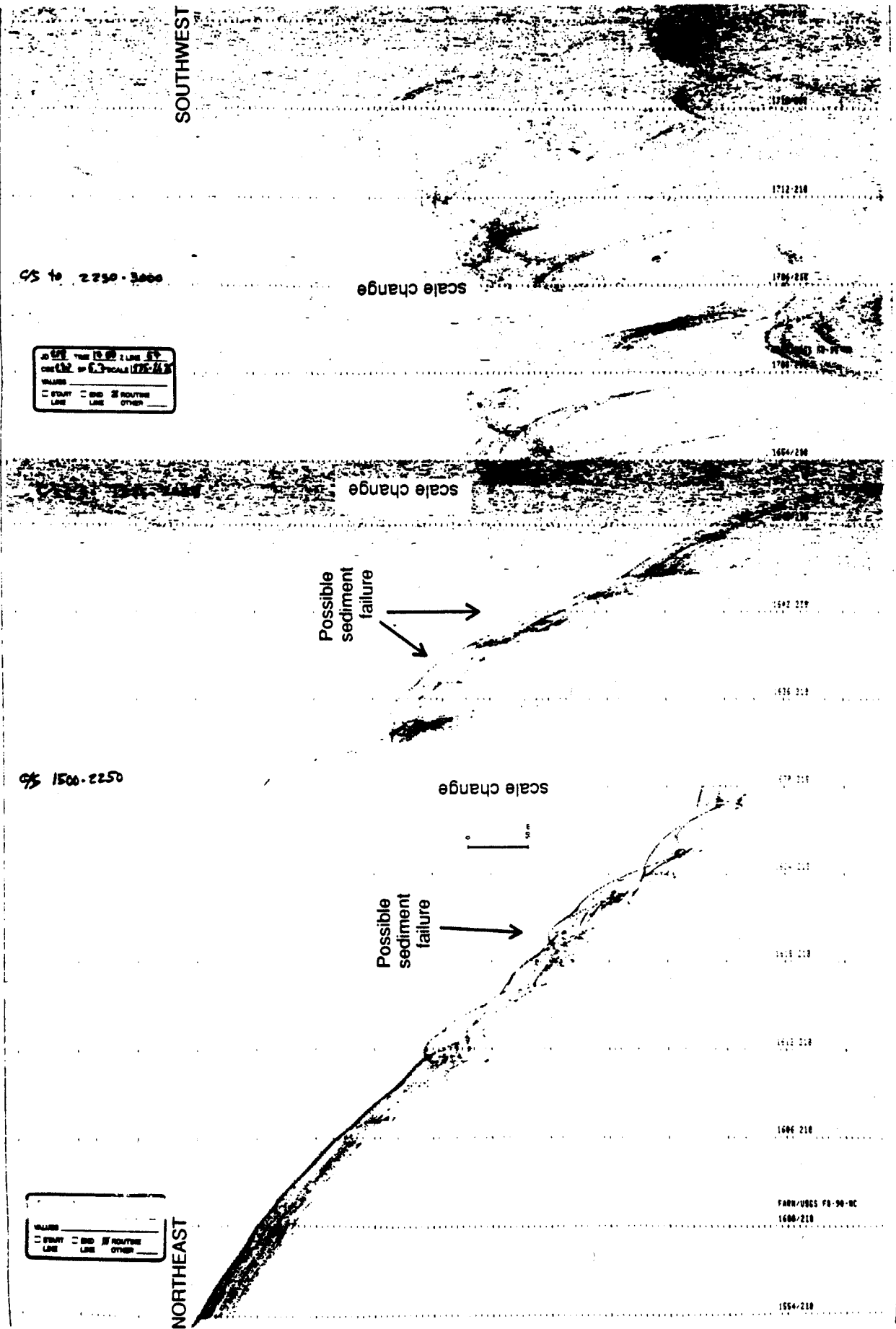


Figure 7b

Line 22



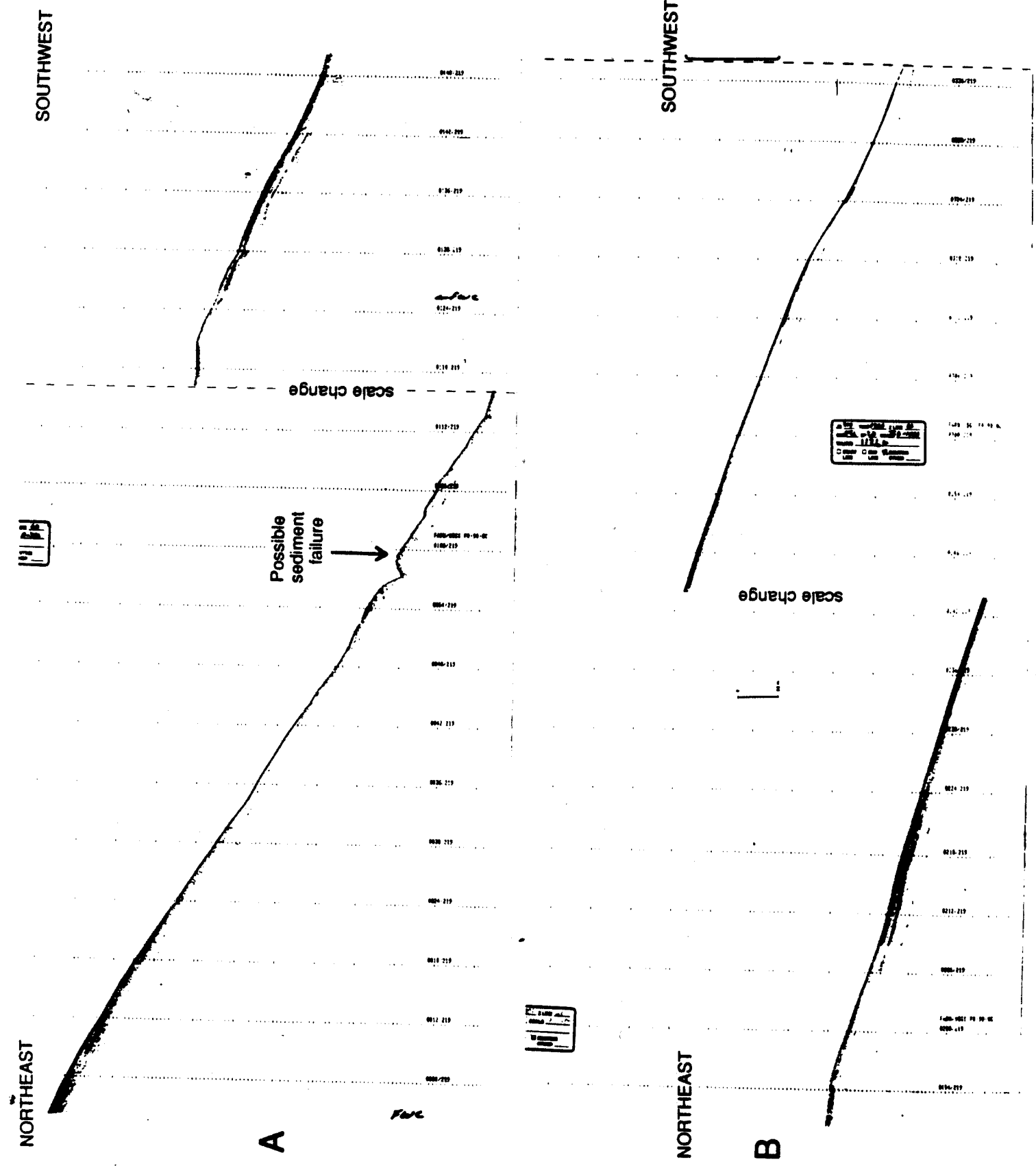


Line 57

Figure 8

Figure 9

Line 60



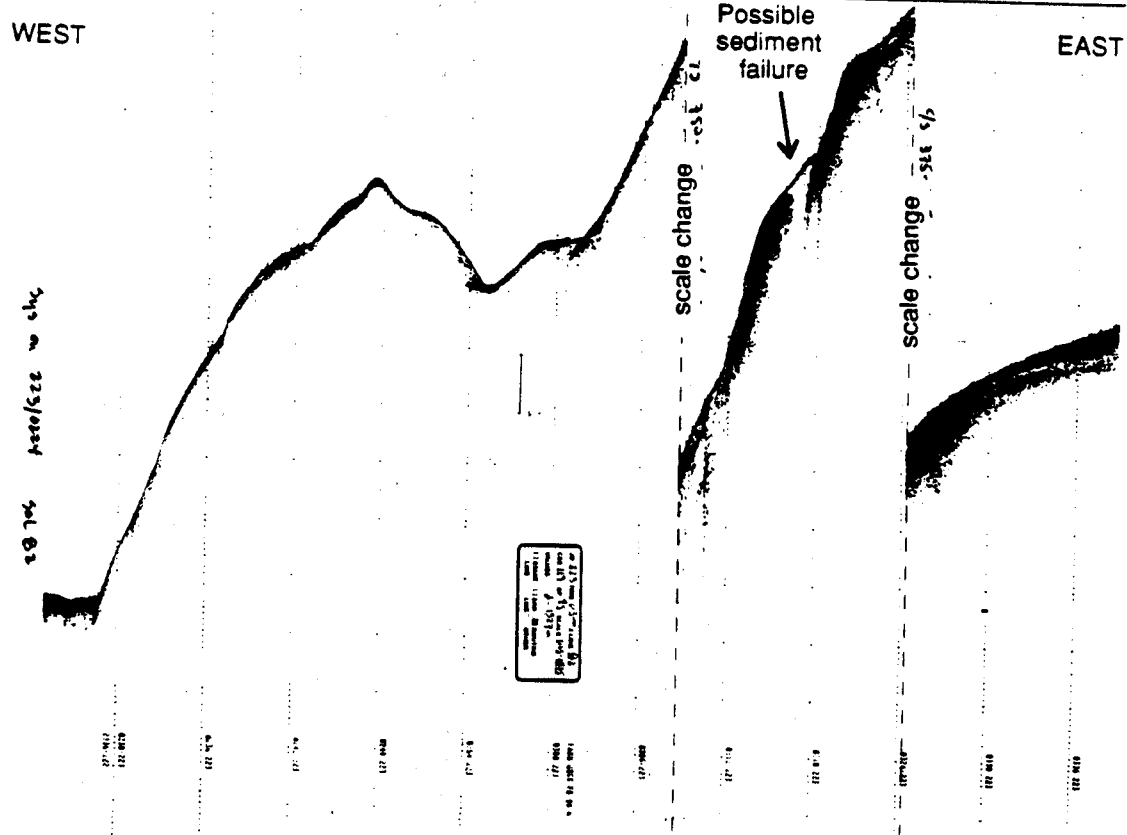
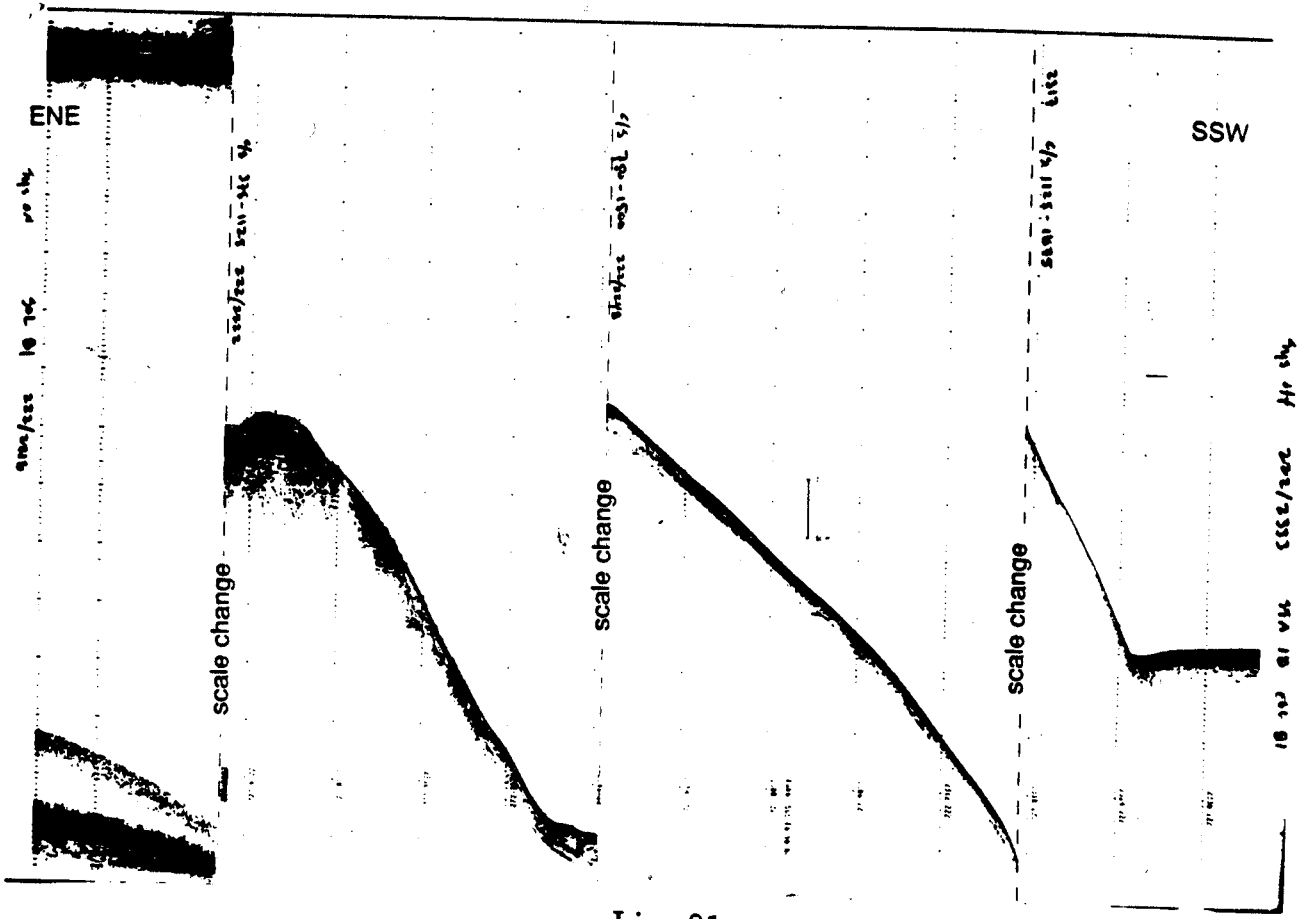


Figure 10

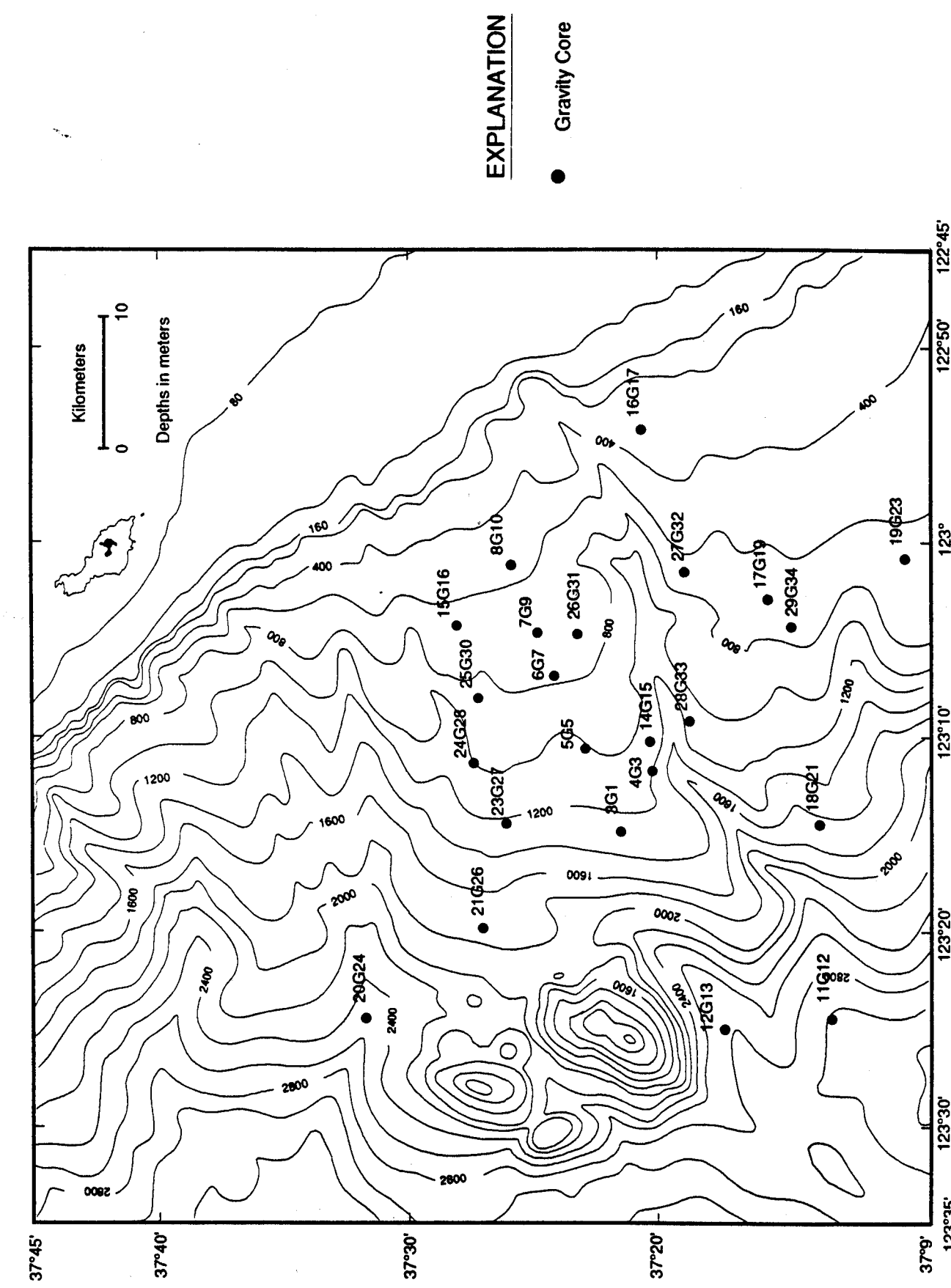


Figure 11

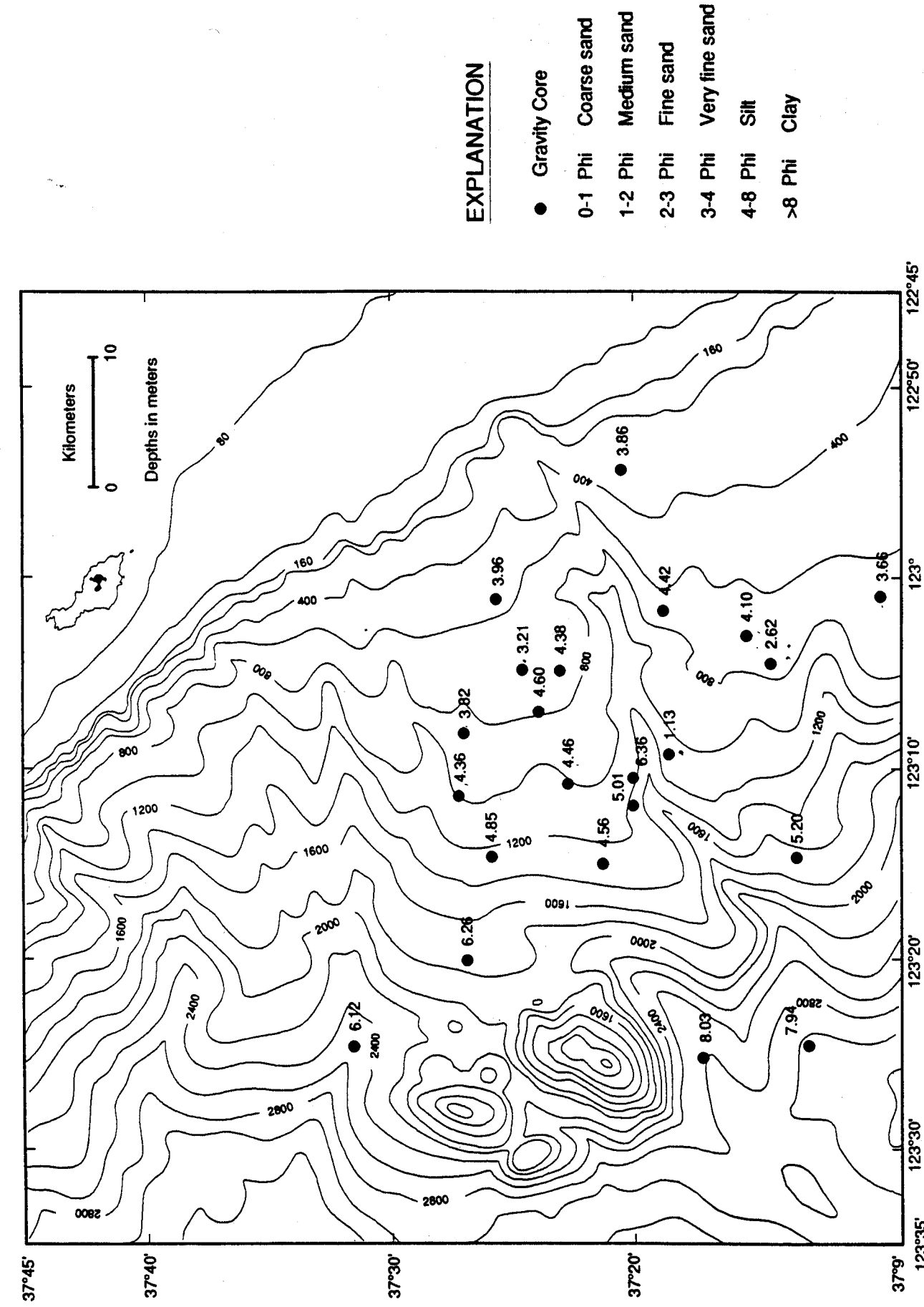
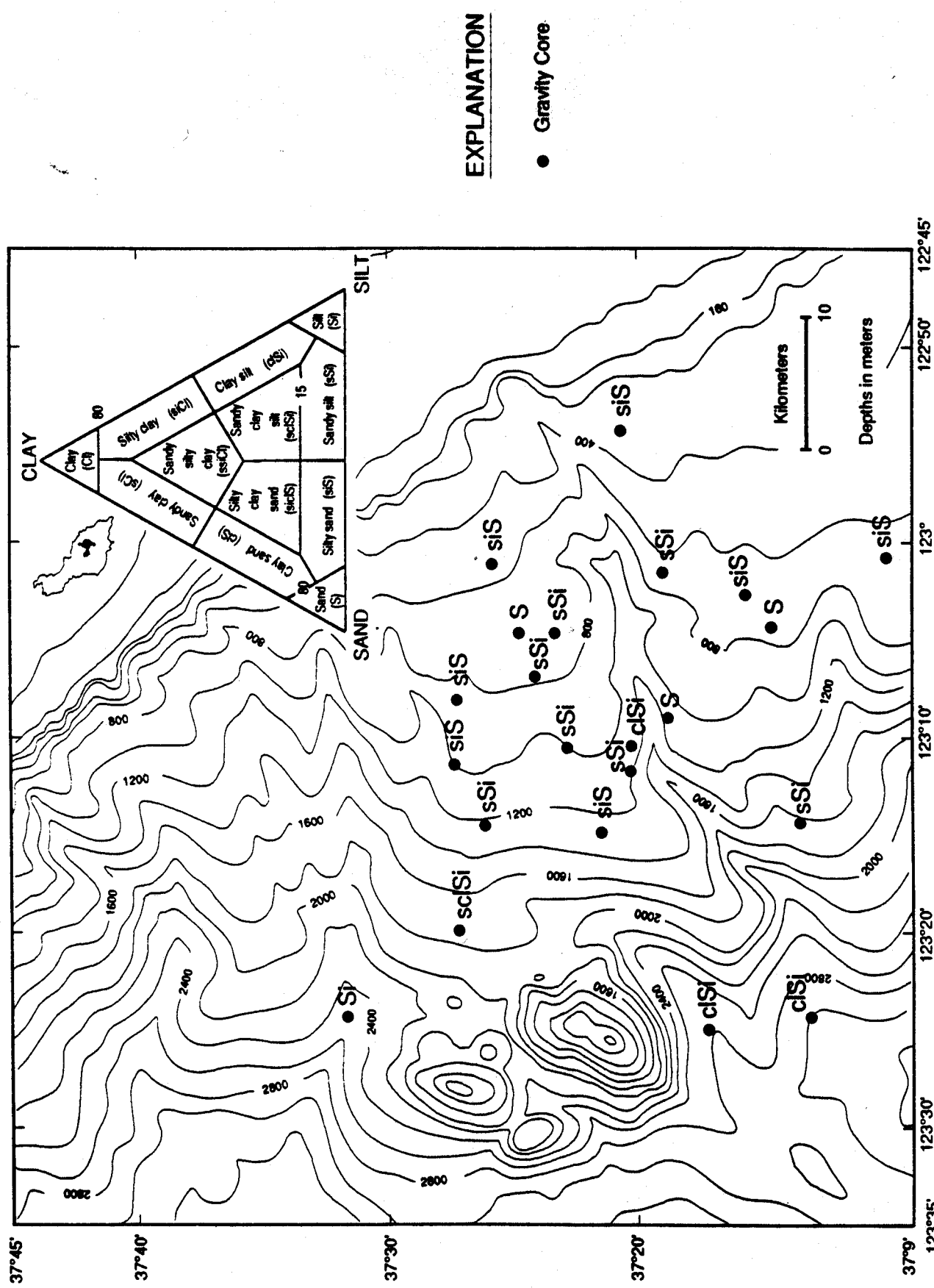


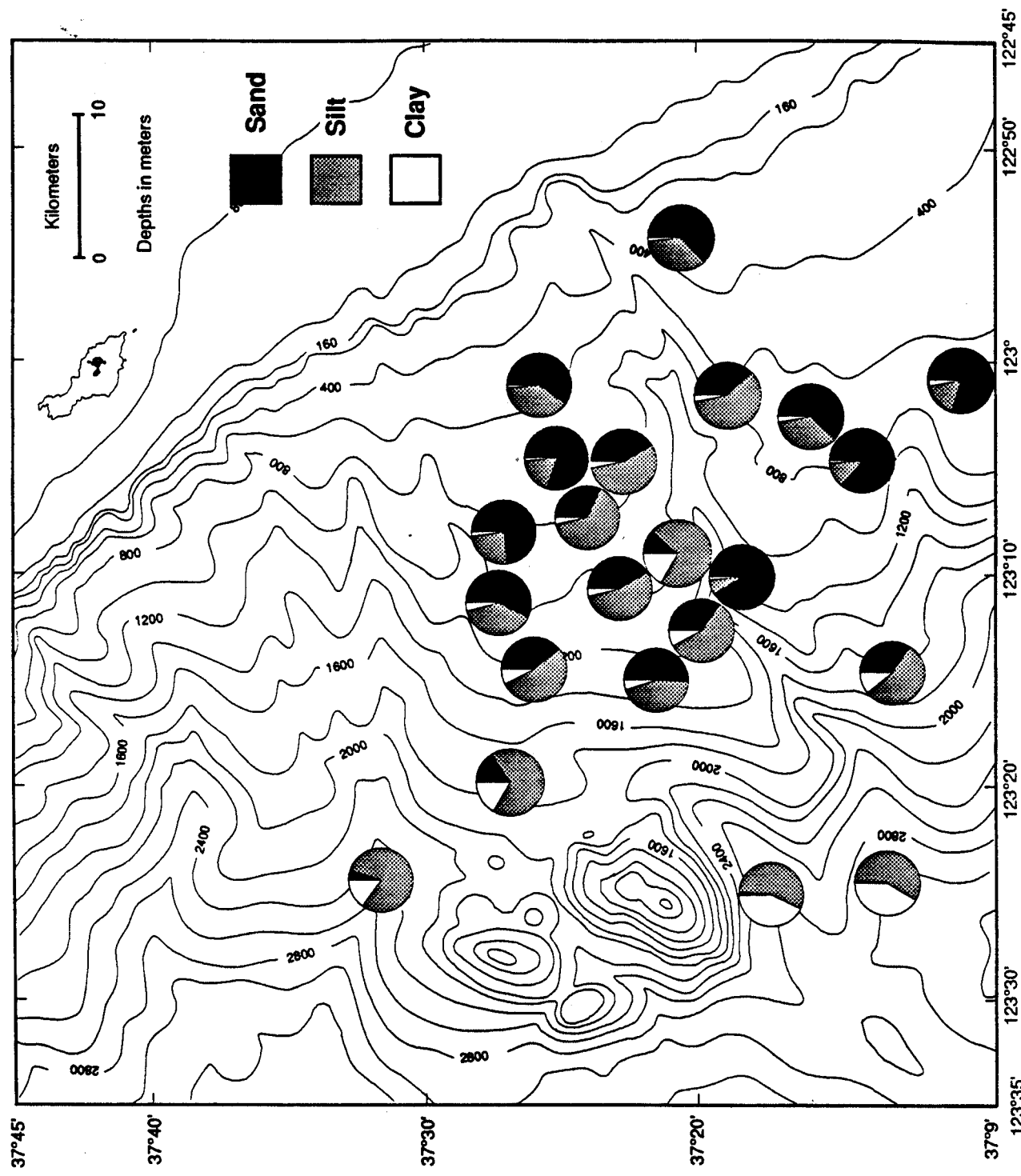
Figure 12

Mean grain size of surface sediment (phi units)



Surface sediment texture (Shepard, 1954)

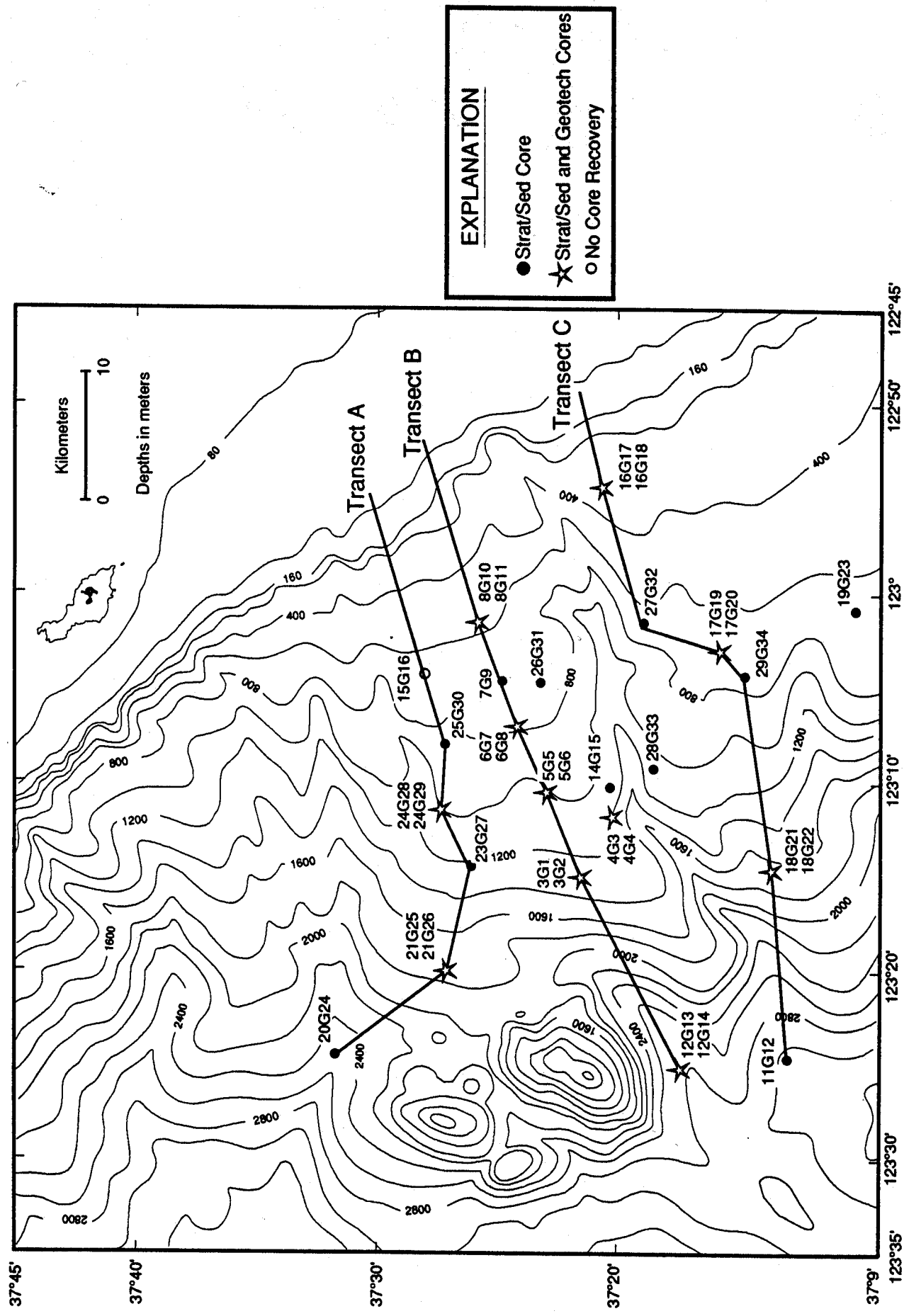
Figure 13



Surface sediment pie charts

Figure 14

Figure 15

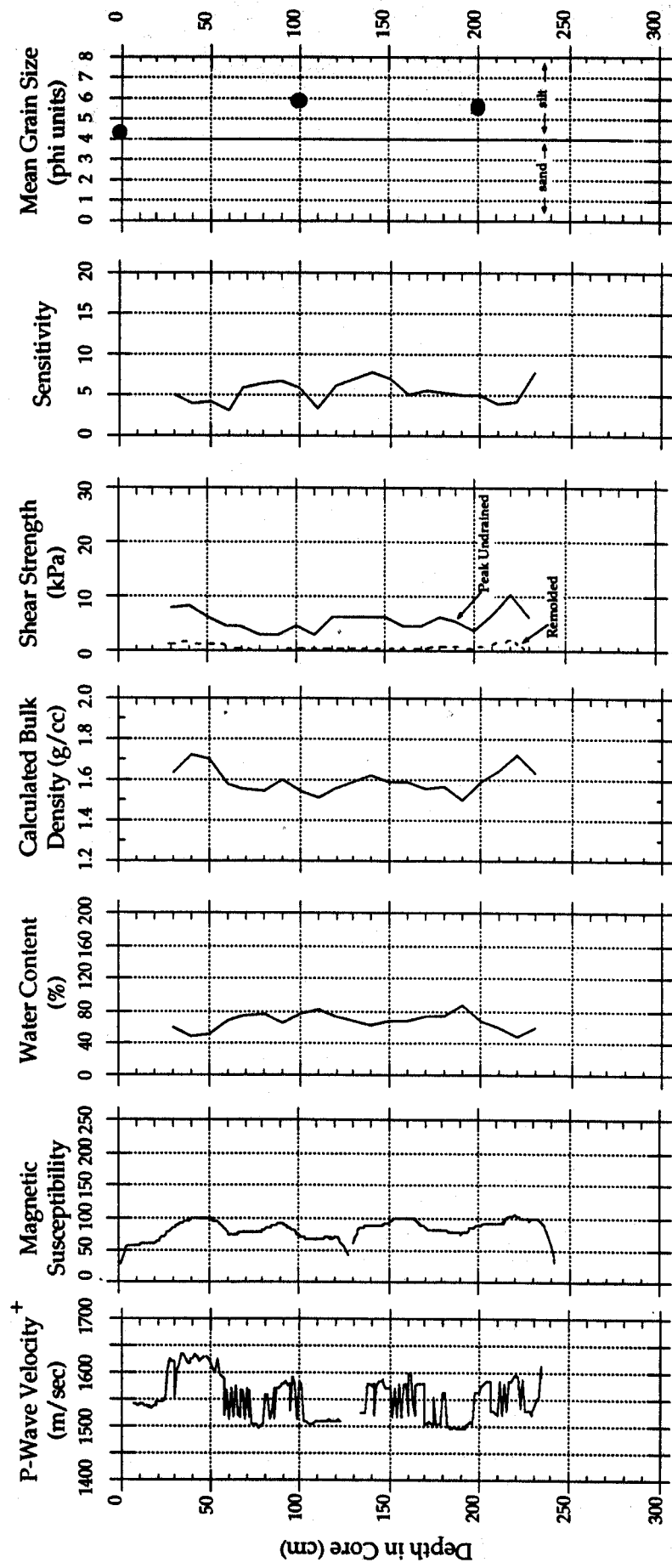


Cruise ID: F8-90-NC

Core: 3G1

FARALLON SLOPE STUDY

Transect B
Water Depth: 1260 m
Environment: Middle Slope



+ Calibration Incomplete

Preliminary Data: Not for Release or Publication

Figure 16

F8-90-NC
Transect B

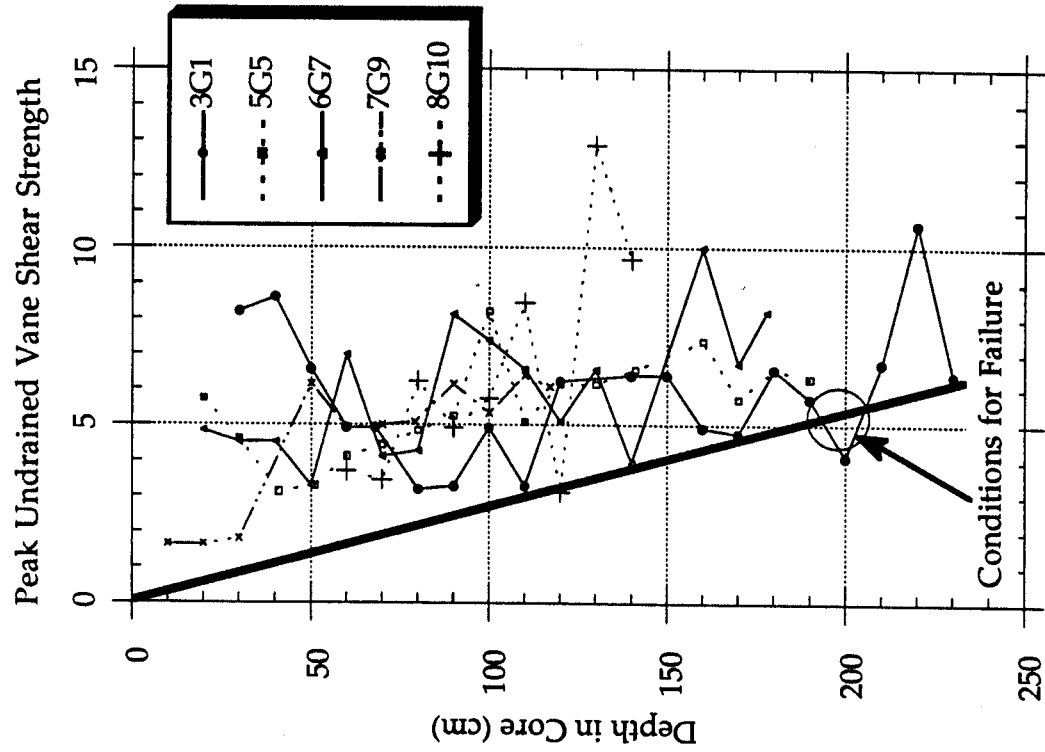
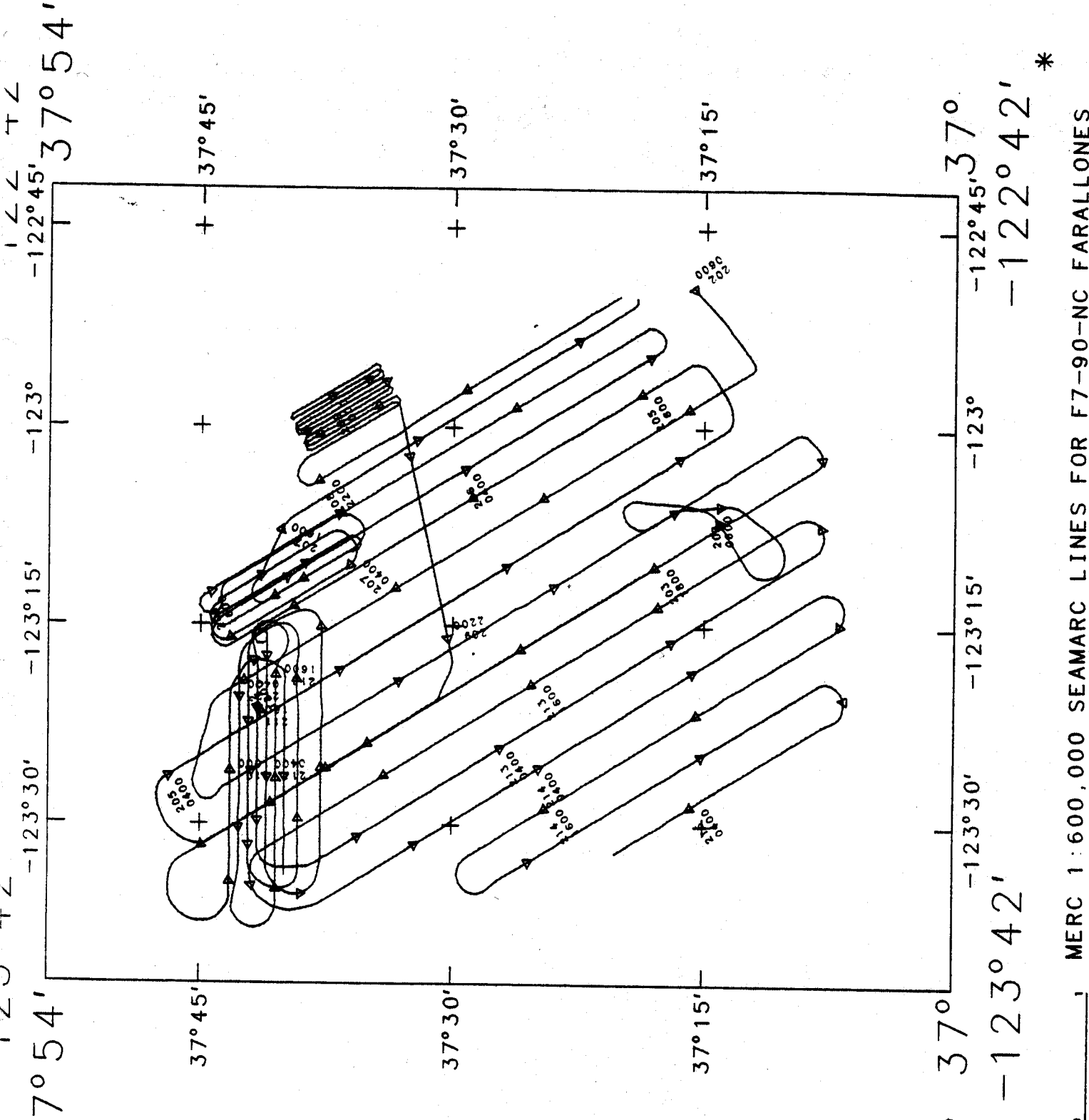


Figure 17

Table 1. F8-90-NC Core Data

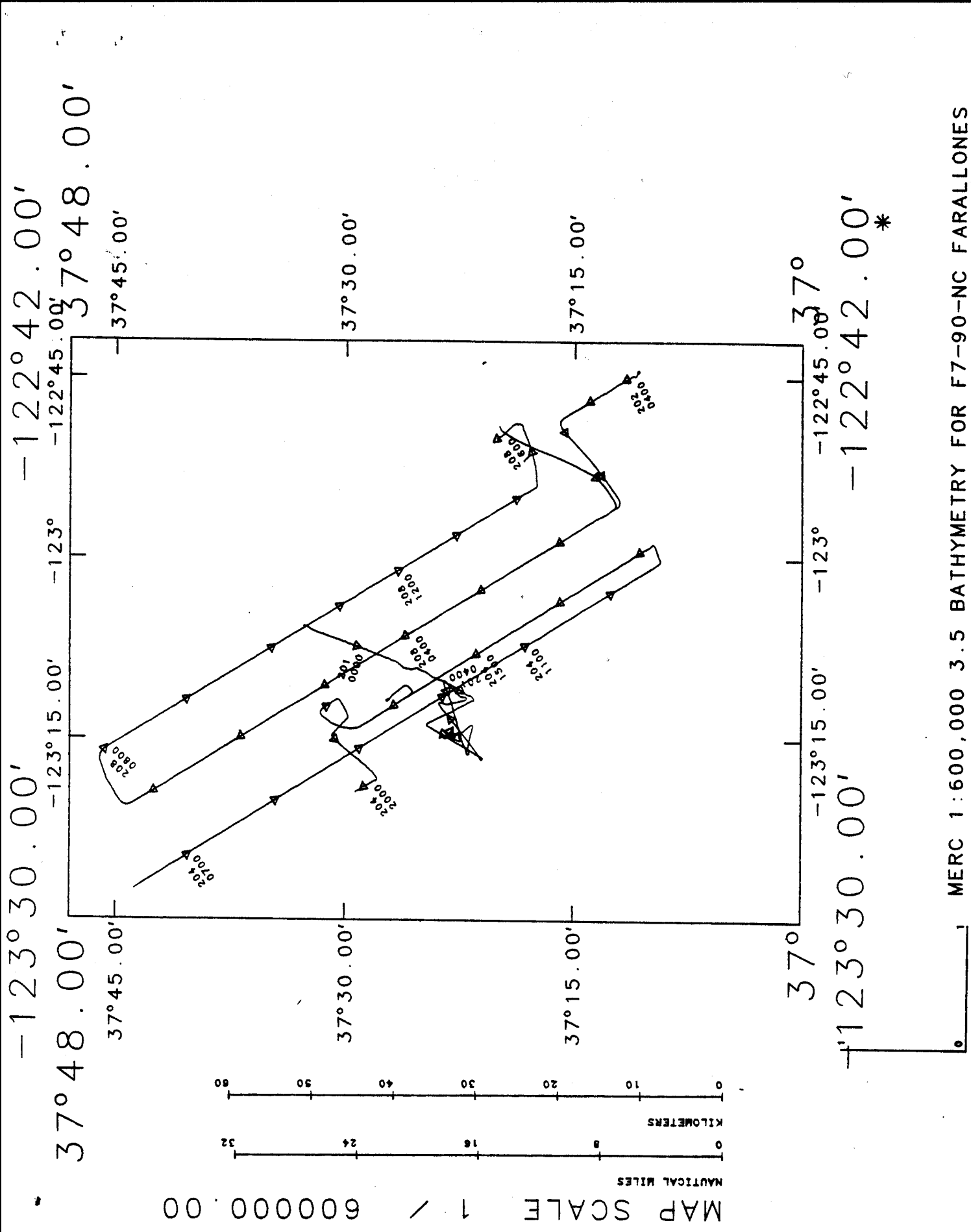
Core ID	Type	Recovery (cm)	Water Depth (m)	Environment	Transsect	Latitude	Longitude
3G1	SS	241	1260	Middle Slope	B	37°21'37"	-123°14.87'
3G2	GT	267	1250	Middle Slope	B	37°21'37"	-123°14.79'
4G3	SS	230	1545	Canyon Flank/Floor	-	37°20.09'	-123°11.86'
4G4	GT	232	1545	Canyon Flank/Floor	-	37°20.18'	-123°11.81'
5G5	SS	198	960	Middle Slope	B	37°22.81'	-123°10.70'
5G6	GT	279	967	Middle Slope	B	37°22.78'	-123°10.74'
6G7	SS	182	795	Upper Slope	B	37°24.00'	-123°06.99'
6G8	GT	179	800	Upper Slope	B	37°24.00'	-123°07.00'
7G9	SS	121	716	Upper Slope	B	37°24.68'	-123°04.74'
8G10	SS	161	537	Upper Slope	B	37°25.70'	-123°01.20'
8G11	GT	239	540	Upper Slope	B	37°25.66'	-123°01.26'
11G12	SS	197	3120	Base-of-Slope	C	37°12.97'	-123°24.52'
12G13	SS	235	2805	Base-of-Slope	B	37°17.24'	-123°25.09'
12G14	GT	280	2710	Base-of-Slope	B	37°17.29'	-123°25.07'
14G15	SS	163	1540	Canyon Flank/Floor	-	37°20.16'	-123°10.41'
15G16	-	NR	600	Upper Slope	A	37°27.93'	-123°04.34'
16G17	SS	122	280	Upper Slope	C	37°20.56'	-122°54.34'
16G18	GT	143	276	Upper Slope	C	37°20.70'	-122°54.47'
17G19	SS	263	670	Upper Slope	C	37°15.49'	-123°03.05'
17G20	GT	216	665	Upper Slope	C	37°15.57'	-123°03.00'
18G21	SS	163	1605	Lower Slope	C	37°13.45'	-123°14.63'
18G22	GT	269	1604	Lower Slope	C	37°13.47'	-123°14.58'
19G23	SS	51	630	Upper Slope	-	37°09.96'	-123°00.88'
20G24	SS	209	2495	Base-of-Slope	A	37°31.65'	-123°24.50'
21G25	SS	116	1720	Lower Slope	A	37°27.01'	-123°20.03'
21G26	GT	145	1720	Lower Slope	A	37°26.93'	-123°20.00'
23G27	SS	217	1378	Middle Slope	A	37°25.99'	-123°14.60'
24G28	SS	258	970	Middle Slope	A	37°27.27'	-123°11.46'
24G29	GT	277	970	Middle Slope	A	37°27.26'	-123°11.38'
25G30	SS	241	808	Middle Slope	A	37°27.09'	-123°08.11'
26G31	SS	223	728	Upper Slope	-	37°23.12'	-123°04.78'
27G32	SS	285	638	Upper Slope	C	37°18.83'	-123°01.70'
28G33	SS	27	1050	Lower Slope	B	37°18.65'	-123°09.23'
29G34	SS	128	685	Upper Slope	C	37°14.49'	-123°04.45'

APPENDIX II



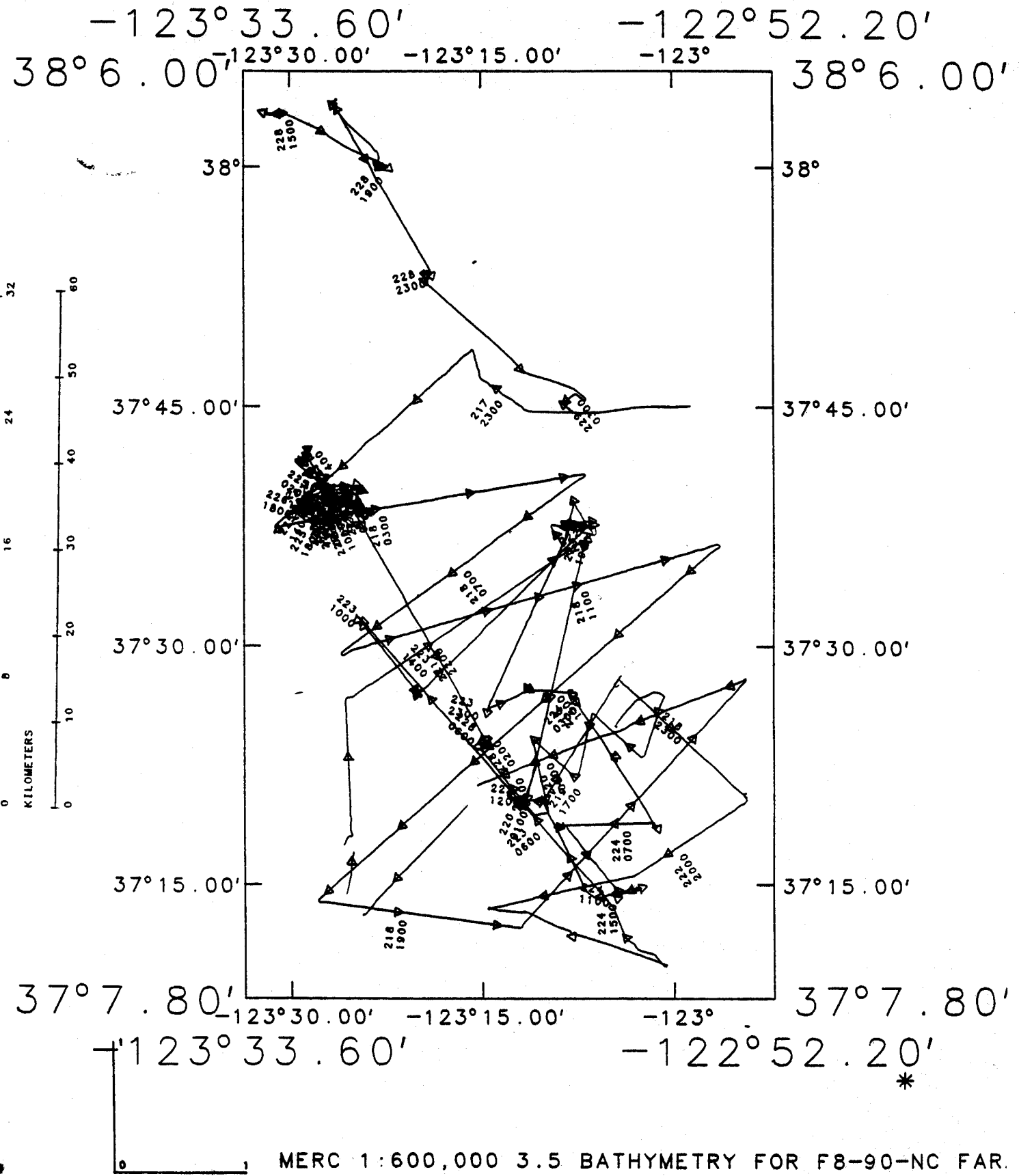
MERC 1 : 600,000 SEAMARC LINES FOR F7-90-NC FARALLONES

APPENDIX III

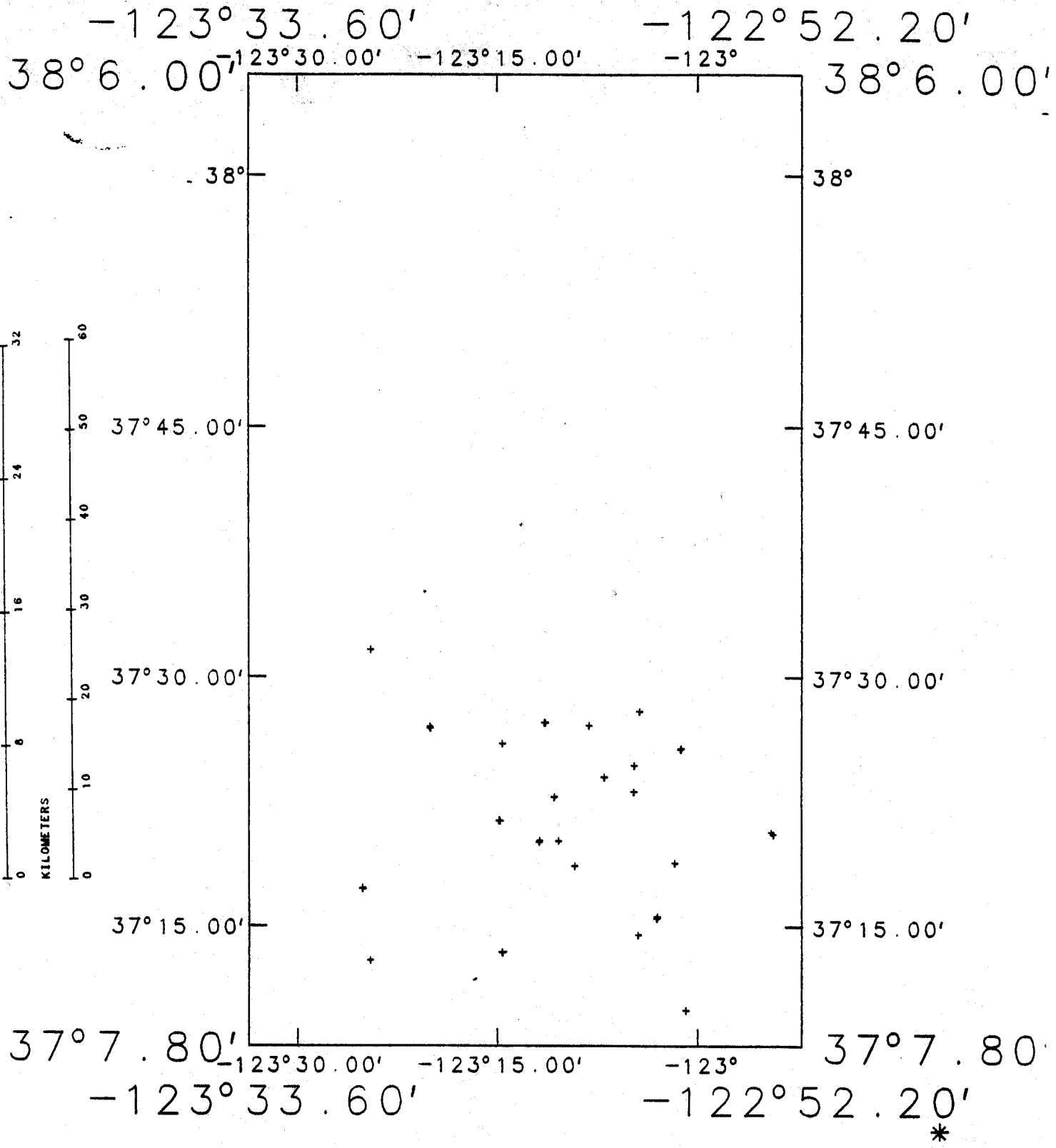


MERC 1 : 600,000 3.5 BATHYMETRY FOR F7-90-NC FARALLONES

APPENDIX IV

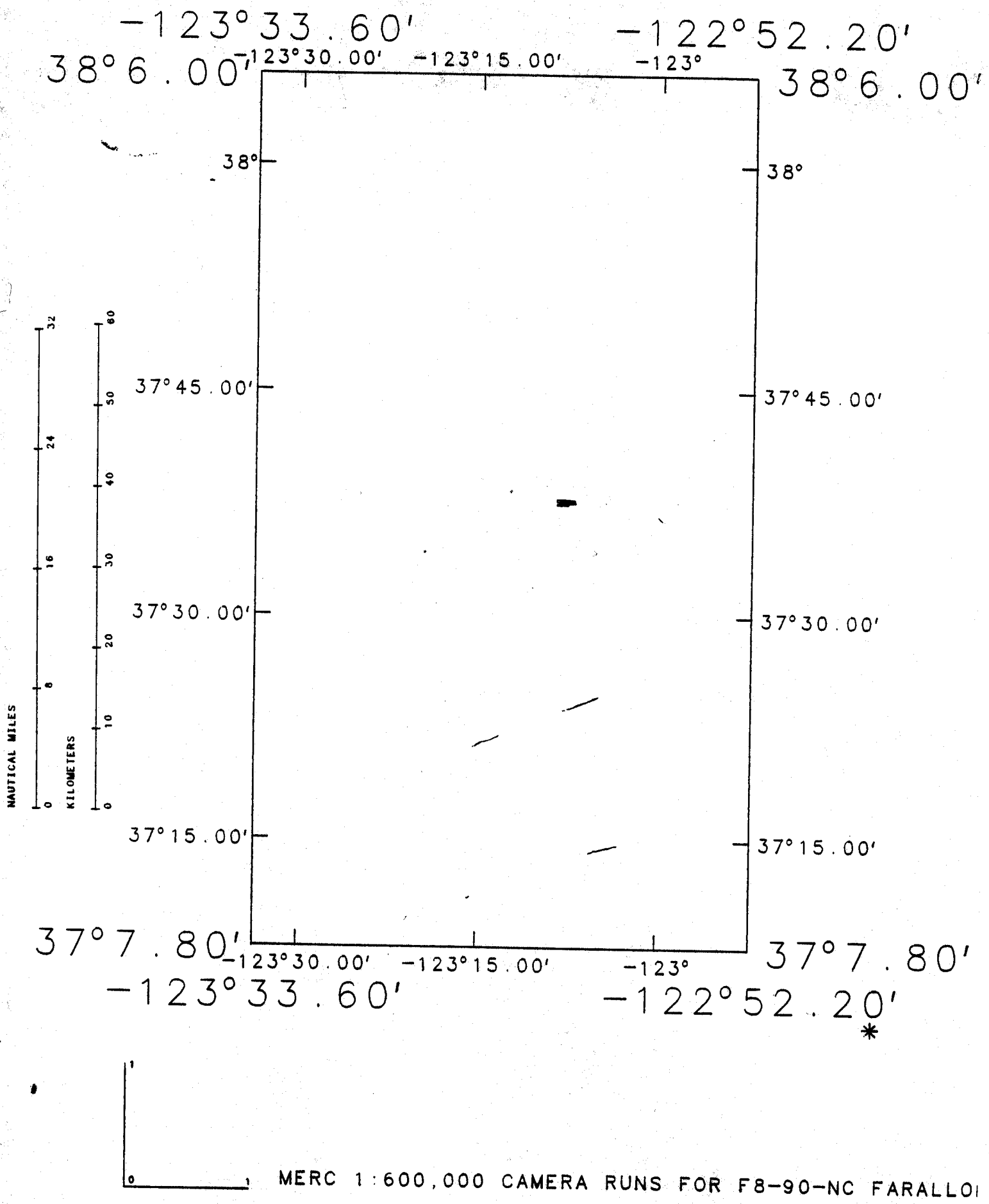


APPENDIX V



MERC 1:600,000 SAMPLE LOCATIONS FOR F8-90-NC F

APPENDIX VI



APPENDIX VII

F890NC Sediment Data

Sample no.	Latitude	Longitude	Depth (meters)	Texture	Percent Gravel	Percent Sand	Percent Silt	Percent Clay	Percent Mud	Sand/Mud Ratio
3g1-surf	37.35617	-123.24783	1260	silty Sand	0.00	51.24	43.76	4.99	46.76	1.05
3g1-100	37.35617	-123.24783	1260	clay Silt	0.00	10.84	73.96	15.20	89.16	0.12
3g1-200	37.35617	-123.24783	1260	sandy Silt	0.00	16.01	71.03	12.96	83.99	0.19
3g1-200dp	37.35617	-123.24783	1260	sandy Silt	0.00	14.59	71.76	13.65	85.41	0.17
3g2-surf	37.35617	-123.24650	1250	silty Sand	0.00	49.67	44.72	5.61	50.33	0.99
4g3-surf	37.33483	-123.19767	1545	sandy Silt	0.00	35.27	56.68	8.05	64.73	0.54
4g4-surf	37.33630	-123.19683	1545	sandy Silt	0.00	23.28	65.63	11.09	76.72	0.30
5g5-surf	37.38017	-123.17833	960	sandy Silt	0.00	41.41	54.95	3.65	58.59	0.71
5g5-100	37.38017	-123.17833	960	clay Silt	0.00	12.36	74.67	12.97	87.64	0.14
5g5-197	37.38017	-123.17833	960	clay Silt	0.00	3.09	76.89	20.02	96.91	0.03
5g6-surf	37.37967	-123.17900	967	sandy Silt	0.00	39.83	56.95	3.22	60.17	0.66
6g7-surf	37.40000	-123.11650	795	sandy Silt	0.00	32.38	64.24	3.37	67.62	0.48
6g7-100	37.40000	-123.11650	795	Silt	0.00	8.81	80.96	10.23	91.19	0.10
6g8-surf	37.40000	-123.11667	800	sandy Silt	0.00	39.63	56.89	3.47	60.37	0.66
7g9-surf	37.41133	-123.07900	716	Sand	0.00	80.68	18.08	1.25	19.32	4.17
7g9-100	37.41133	-123.07900	716	Silt	0.00	6.99	83.35	9.66	93.01	0.08
8g10-surf	37.42833	-123.02000	537	silty Sand	0.00	59.75	38.93	1.32	40.25	1.48
8g10-surfdp	37.42833	-123.02000	537	silty Sand	0.00	61.80	36.90	1.30	38.20	1.62
8g10-100	37.42833	-123.02000	537	Silt	0.00	11.17	81.25	7.58	88.83	0.13
8g11-surf	37.42767	-123.02100	540	silty Sand	0.00	63.14	35.87	0.99	36.86	1.71
11g12-surf	37.21617	-123.40876	3120	clay Silt	0.00	1.07	57.99	40.95	98.93	0.01
11g12-100	37.21617	-123.40876	3120	clay Silt	0.00	2.08	53.50	44.42	97.92	0.02
12g13-surf	37.28733	-123.41817	2805	clay Silt	0.00	1.39	55.93	42.68	98.61	0.01
12g14-surf	37.28817	-123.41783	2710	clay Silt	0.00	1.84	60.98	37.18	98.16	0.02
14g15-surf	37.33600	-123.17350	1540	clay Silt	0.00	10.84	72.27	16.90	89.16	0.12
16g17-surf	37.34267	-122.90567	280	silty Sand	0.00	63.51	35.17	1.32	36.49	1.74
16g17-100	37.34267	-122.90567	280	sandy Silt	0.00	30.04	65.18	4.78	69.96	0.43
16g18-surf	37.34500	-122.90783	285	silty Sand	0.00	71.28	27.62	1.10	28.72	2.48
17g19-surf	37.25817	-123.05083	670	silty Sand	0.00	61.70	35.35	2.94	38.30	1.61
17g19-100	37.25817	-123.05083	670	sandy Silt	0.00	14.63	72.61	12.76	85.37	0.17

F890NC Sediment Data

Sample no.	Latitude	Longitude	Depth (meters)	Sediment Texture	Percent Gravel	Percent Sand	Percent Silt	Percent Clay	Percent Mud	Sand/Mud Ratio
17g19-200	37.25817	-123.05083	670	sandy Silt	0.00	13.07	78.58	8.36	86.93	0.15
17g20-surf	37.25950	-123.05000	665	silty Sand	0.00	64.78	32.89	2.32	35.22	1.84
17g20-surfdp	37.25950	-123.05000	665	silty Sand	0.00	64.50	33.28	2.22	35.50	1.82
18g21-surf	37.22417	-123.24383	1605	sandy Silt	0.00	34.89	54.25	10.86	65.11	0.54
18g21-100	37.22417	-123.24383	1605	clay Silt	0.00	9.26	71.11	19.63	90.74	0.10
18g22-surf	37.22450	-123.24300	1604	sandy Silt	0.00	31.91	58.20	9.90	68.09	0.47
18g22-surfdp	37.22450	-123.24300	1604	sandy Silt	0.00	31.41	59.55	9.03	68.59	0.46
19g23-surf	37.16600	-123.01467	630	silty Sand	0.00	79.63	17.39	2.98	20.37	3.91
20g24-surf	37.52750	-123.40833	2495	Silt	0.00	4.97	80.40	14.63	95.03	0.05
20g24-100	37.52750	-123.40833	2495	clay Silt	0.00	2.48	63.85	33.66	97.52	0.03
21g25-surf	37.45017	-123.33383	1720	sandy clay Si	0.00	15.92	67.51	16.57	84.08	0.19
21g25-100	37.45017	-123.33383	1720	clay Silt	0.00	14.76	69.25	15.99	85.24	0.17
21g26-surf	37.44883	-123.33333	1720	sandy Silt	0.00	19.00	66.75	14.24	81.00	0.23
23g27-surf	37.43317	-123.24333	1378	sandy Silt	0.00	39.35	53.58	7.06	60.65	0.65
23g27-100	37.43317	-123.24333	1378	sandy Silt	0.00	46.93	50.18	2.88	53.07	0.88
24g28-surf	37.45450	-123.19100	970	silty Sand	0.00	57.71	38.07	4.22	42.29	1.36
24g28-100	37.45450	-123.19100	970	clay Silt	0.00	10.92	75.51	13.57	89.08	0.12
24g28-200	37.45450	-123.19100	970	clay Silt	0.00	4.02	75.60	20.38	95.98	0.04
24g29-surf	37.45433	-123.18967	970	silty Sand	0.00	48.07	46.47	5.46	51.93	0.93
25g30-surf	37.45150	-123.13517	808	silty Sand	0.00	73.57	24.48	1.95	26.43	2.78
26g31-surf	37.38533	-123.07967	728	sandy Silt	0.00	41.87	55.09	3.04	58.13	0.72
26g31-100	37.38533	-123.07967	728	clay Silt	0.00	10.14	76.14	13.72	89.86	0.11
26g31-200	37.38533	-123.07967	728	Silt	0.00	3.41	83.36	13.23	96.59	0.04
27g32-surf	37.31383	-123.02833	638	sandy Silt	0.00	37.58	59.72	2.70	62.42	0.60
27g32-surfdp	37.31383	-123.02833	638	sandy Silt	0.00	38.72	58.74	2.54	61.28	0.63
27g32-100	37.31383	-123.02833	638	Silt	0.00	3.10	88.90	8.00	96.90	0.03
27g32-200	37.31383	-123.02833	638	Silt	0.00	11.60	81.03	7.37	88.40	0.13
28g33-surf	37.31083	-123.15383	1050	Sand	0.00	91.94	6.95	1.11	8.06	11.40
29g34-surf	37.24150	-123.07417	685	Sand	0.00	86.27	12.56	1.17	13.73	6.28
29g34-100	37.24150	-123.07417	685	silty Sand	0.00	66.80	29.91	3.29	33.20	2.01

Sample no.	1st Moment	2nd Moment	3rd Moment	4th Moment	Mean	Median	Sorting	Skewness	Kurtosis
3g1-surf	4.56	1.84	1.83	7.07	4.38	3.96	1.46	0.54	1.22
3g1-100	5.99	2.04	1.01	3.95	5.90	5.51	1.82	0.31	0.97
3g1-200	5.78	2.05	1.09	4.02	5.63	5.25	1.82	0.33	0.93
3g1-200dp	5.79	2.02	1.10	4.08	5.62	5.19	1.76	0.37	0.90
3g2-surf	4.50	1.79	2.00	7.48	4.36	4.01	1.41	0.57	1.45
4g3-surf	5.01	1.93	1.48	5.42	4.87	4.52	1.72	0.38	1.03
4g4-surf	5.59	2.02	1.02	4.18	5.37	5.20	1.85	0.20	0.91
5g5-surf	4.46	1.44	2.36	10.73	4.24	4.11	1.11	0.38	1.76
5g5-100	6.03	2.06	1.10	4.08	5.83	5.54	1.80	0.29	1.16
5g5-197	6.70	2.01	0.87	3.74	6.57	6.37	1.82	0.25	1.09
5g6-sur	4.48	1.40	2.33	10.79	4.28	4.15	1.10	0.36	1.77
6g7-surf	4.60	1.48	2.43	11.07	4.43	4.24	1.15	0.40	1.97
6g7-100	5.65	1.82	1.55	5.56	5.53	5.05	1.51	0.49	1.09
6g8-surf	4.42	1.44	2.45	11.56	4.17	4.18	1.10	0.22	1.45
7g9-surf	3.21	1.49	1.18	8.96	3.25	3.30	1.19	-0.17	4.45
7g9-100	5.86	1.74	1.38	5.50	5.78	5.40	1.46	0.38	1.11
8g10-surf	3.96	1.07	3.14	19.46	3.80	3.75	0.70	0.31	1.11
8g10-surfdp	3.95	1.06	3.30	20.95	3.79	3.73	0.67	0.36	1.06
8g10-100	5.46	1.75	1.55	5.95	5.40	4.99	1.48	0.42	1.26
8g11-surf	3.95	0.96	2.97	23.13	3.83	3.83	0.58	0.16	1.52
11g12-surf	7.94	1.87	0.42	3.17	7.74	7.64	1.69	0.14	1.79
11g12-100	7.95	2.05	0.28	2.71	7.84	7.77	1.88	0.10	1.81
12g13-surf	8.03	1.91	0.33	3.39	7.84	7.66	1.73	0.21	1.87
12g14-surf	7.97	1.91	0.52	3.00	7.78	7.56	1.77	0.23	1.82
14g15-surf	6.36	1.95	1.05	3.89	6.22	5.91	1.79	0.28	1.03
16g17-surf	3.86	1.18	1.90	14.47	3.77	3.71	0.72	0.29	1.19
16g17-100	4.90	1.57	1.76	7.60	4.79	4.48	1.29	0.45	1.33
16g18-surf	3.77	1.09	2.33	18.76	3.66	3.61	0.60	0.28	1.18
17g19-surf	4.10	1.34	2.93	14.70	3.86	3.77	0.92	0.42	1.80
17g19-100	5.80	1.10	4.13	5.66	5.24	5.24	0.34	0.91	

Sample no.	1st Moment	2nd Moment	3rd moment	4th Moment	Mean	Median	Sorting	Skewness	Kurtosis
17g19-200	5.49	1.73	1.50	6.06	5.38	5.07	1.47	0.33	1.31
17g20-surf	3.98	1.28	2.97	17.19	3.77	3.75	0.77	0.31	2.01
17g20-surfdfp	4.00	1.30	2.97	17.03	3.80	3.75	0.78	0.35	1.66
18g21-surf	5.20	2.15	1.18	4.36	5.04	4.53	1.85	0.45	0.88
18g21-100	6.56	2.15	0.76	3.22	6.50	6.32	2.04	0.19	1.11
18g22-surf	5.16	2.21	1.34	4.65	4.82	4.12	1.92	0.60	1.00
18g22-surfdfp	5.19	2.15	1.36	4.91	4.94	4.47	1.84	0.47	0.98
19g23-surf	3.66	1.57	2.31	12.36	3.55	3.39	1.07	0.36	3.22
20g24-surf	6.12	1.98	1.41	4.57	5.94	5.60	1.76	0.39	1.19
20g24-100	7.61	2.02	0.54	3.07	7.37	7.29	1.86	0.15	1.44
21g25-surf	6.26	2.26	0.93	3.46	6.03	5.95	2.17	0.18	1.41
21g25-100	6.28	2.16	0.72	3.45	6.10	6.14	2.02	0.06	1.12
21g26-surf	5.76	2.30	1.09	3.57	5.30	4.31	2.04	0.72	1.03
23g27-surf	4.85	2.02	1.41	5.68	4.70	4.32	1.69	0.44	0.99
23g27-100	4.30	1.51	2.04	10.20	4.10	4.04	1.12	0.31	1.38
24g28-surf	4.36	1.70	2.17	9.01	4.18	3.76	1.29	0.61	1.32
24g28-100	6.06	1.98	1.12	4.31	5.89	5.54	1.76	0.32	1.14
24g28-200	6.84	1.97	0.89	3.70	6.74	6.51	1.82	0.25	1.26
24g29-surf	4.62	1.89	1.89	7.07	4.60	4.02	1.53	0.61	1.13
25g30-surf	3.82	1.33	3.07	16.25	3.63	3.47	0.87	0.48	1.84
26g31-surf	4.38	1.36	2.61	13.15	4.16	4.08	0.98	0.34	1.83
26g31-100	5.91	1.96	1.18	4.25	5.80	5.32	1.71	0.40	0.94
26g31-200	6.15	1.84	1.21	4.58	6.02	5.73	1.55	0.33	0.90
27g32-surf	4.42	1.34	2.39	12.00	4.20	4.16	1.03	0.27	1.69
27g32-surfdfp	4.39	1.36	2.44	12.35	4.18	4.13	1.03	0.27	1.61
27g32-100	5.71	1.61	1.57	6.48	5.58	5.23	1.33	0.47	1.04
27g32-200	5.42	1.67	1.47	5.86	5.35	4.91	1.47	0.45	1.15
28g33-surf	1.13	1.84	2.29	10.28	0.84	1.07	1.44	0.02	1.19
29g34-surf	2.62	1.51	1.80	9.81	2.48	2.33	1.21	0.25	0.82
29g34-100	3.36	2.12	3.23	5.35	3.23	1.84	0.31	0.84	

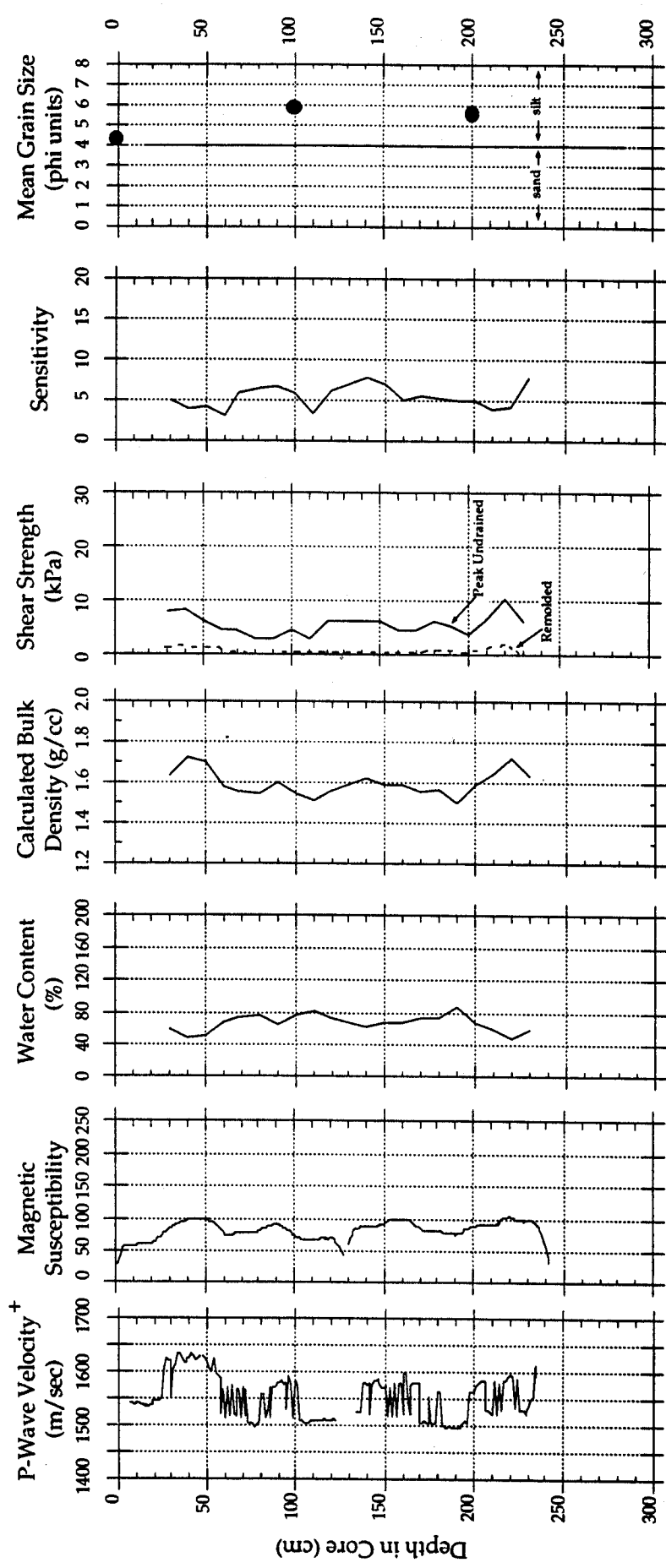
APPENDIX VIII

Cruise ID: F8-90-NC

FARALLON SLOPE STUDY

Core: 3G1

Transect B
Water Depth: 1260 m
Environment: Middle Slope



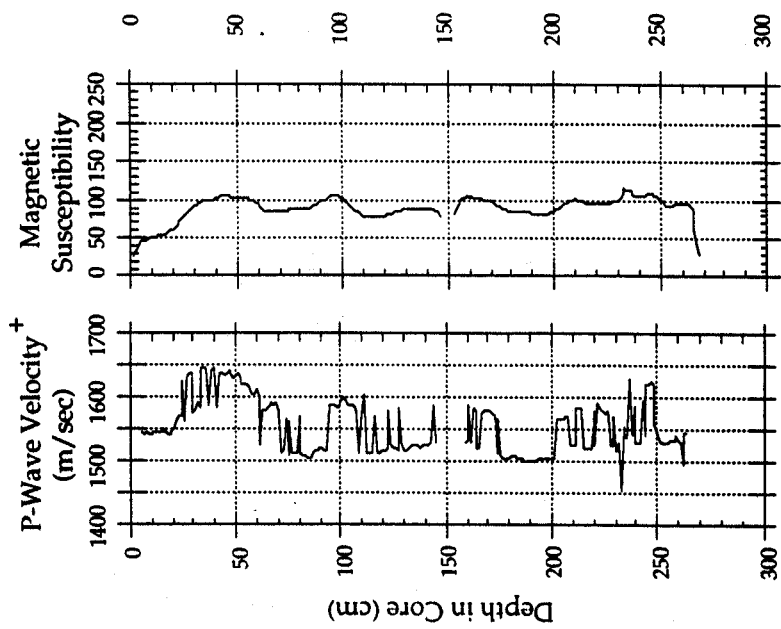
+ Calibration Incomplete

Preliminary Data: Not for Release or Publication

Cruise ID: E8-90-NC
Core: 3G2

FARALLON SLOPE STUDY

Transect B
Water Depth: 1250 m
Environment: Middle Slope



+ Calibration Incomplete

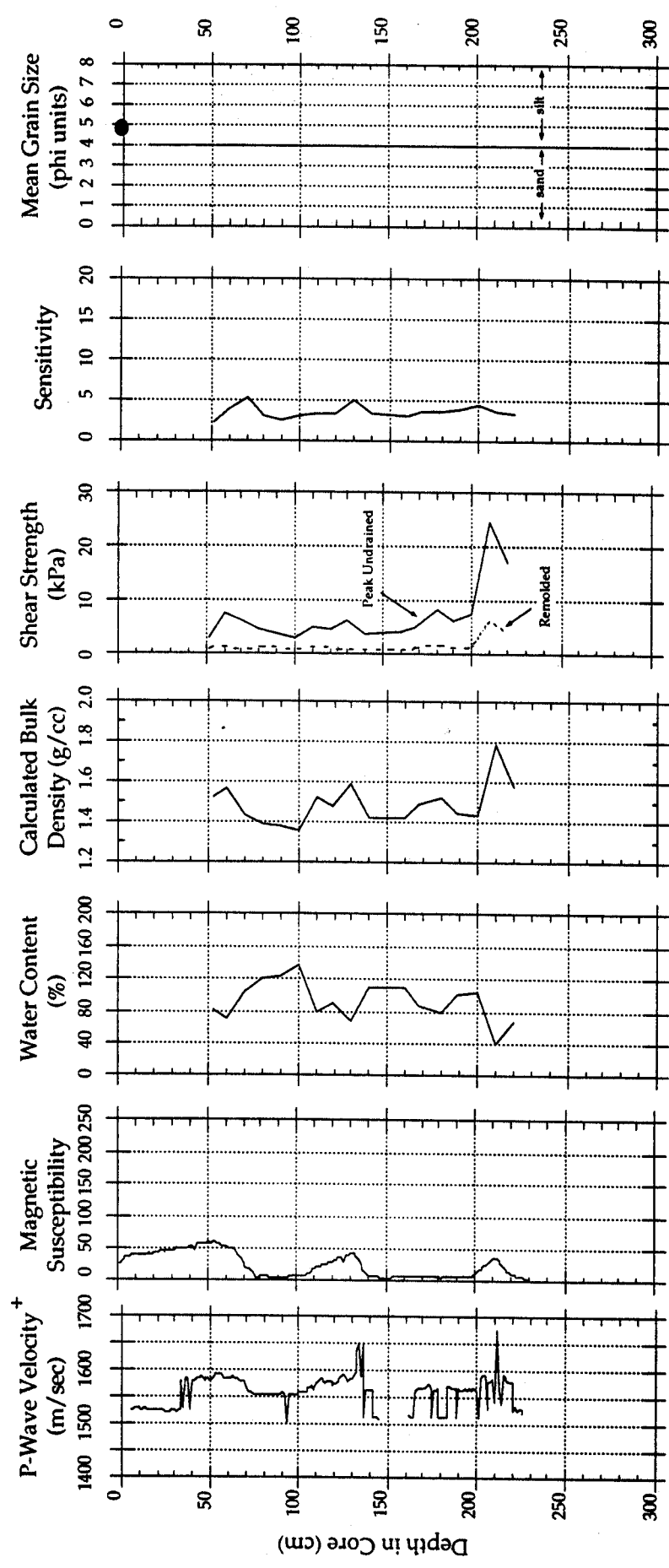
Preliminary Data: Not for Release or Publication

Cruise ID: F8-90-NC

FARALLON SLOPE STUDY

Core: 4G3

Water Depth: 1545 m
Environment: Canyon Flank/Floor



+ Calibration Incomplete

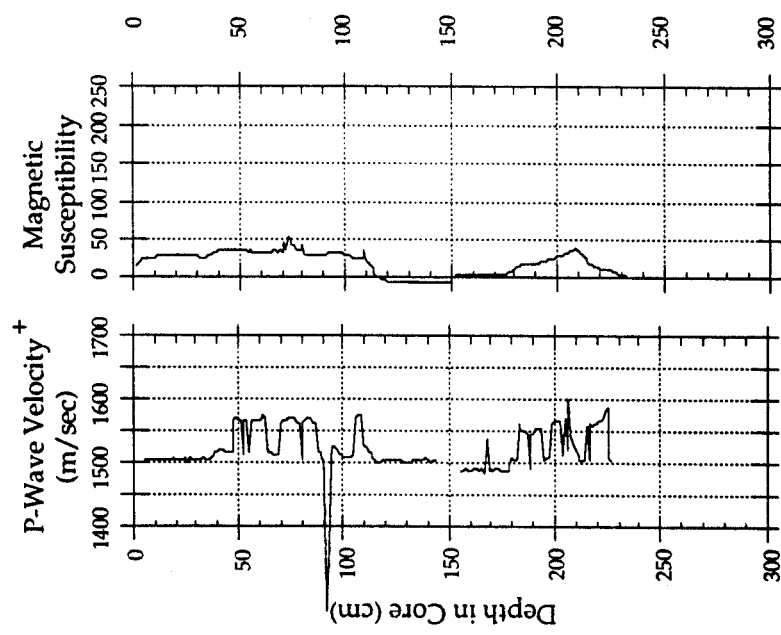
Preliminary Data: Not for Release or Publication

Cruise ID: F8-90-NC

FARALLON SLOPE STUDY

Core: 4G4

Water Depth: 1545 m
Environment: Canyon Axis/Flank



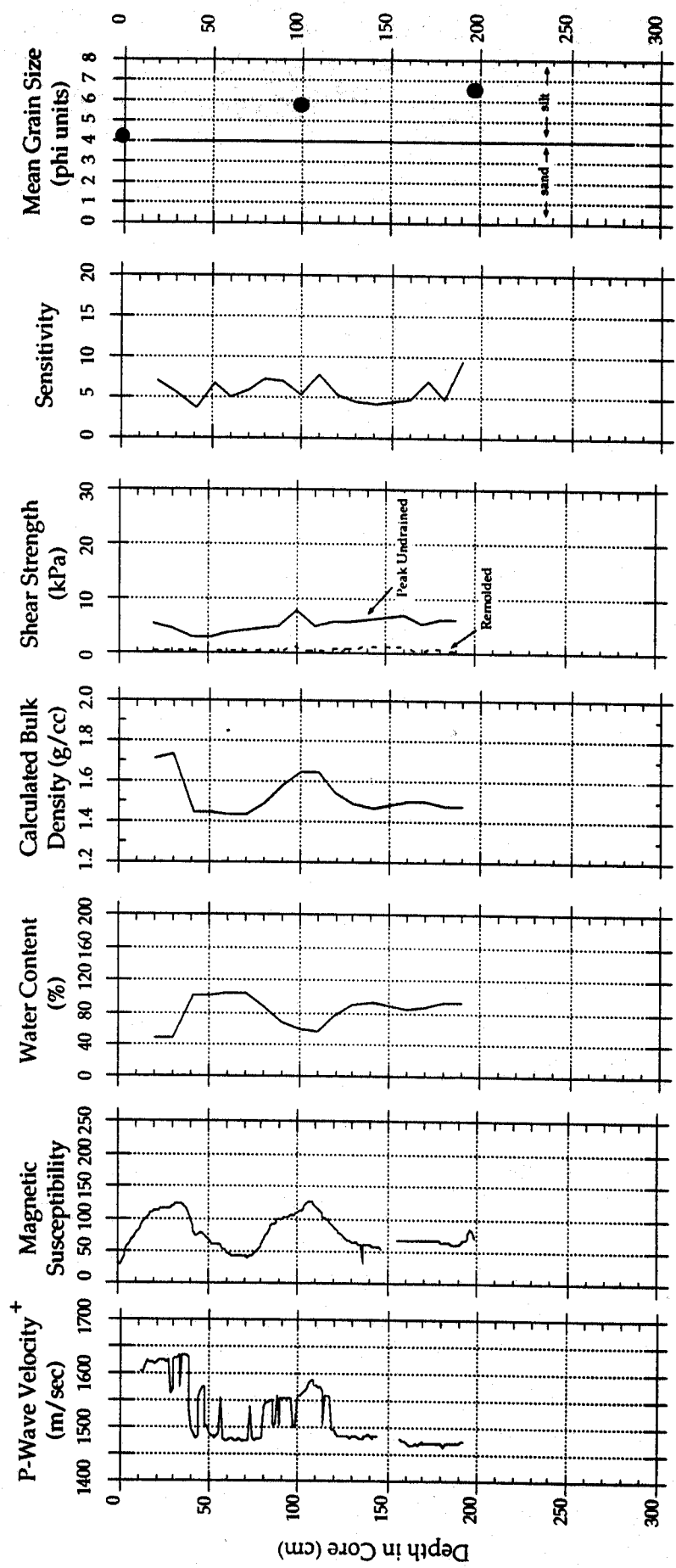
+ Calibration Incomplete

Preliminary Data: Not for Release or Publication

Cruise ID: F8-90-NC
Core: 5G5

FARALLON SLOPE STUDY

Transect B
Water Depth: 960 m
Environment: Middle Slope



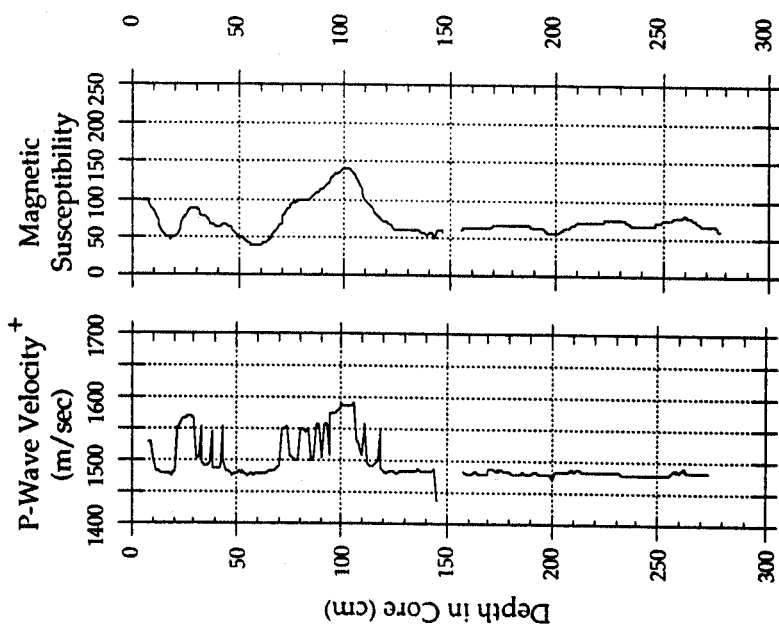
+ Calibration Incomplete

Preliminary Data: Not for Release or Publication

Cruise ID: F8-90-NC
Core: 5G6

FARALLON SLOPE STUDY

Transect B
Water Depth: 967 m
Environment: Middle Slope



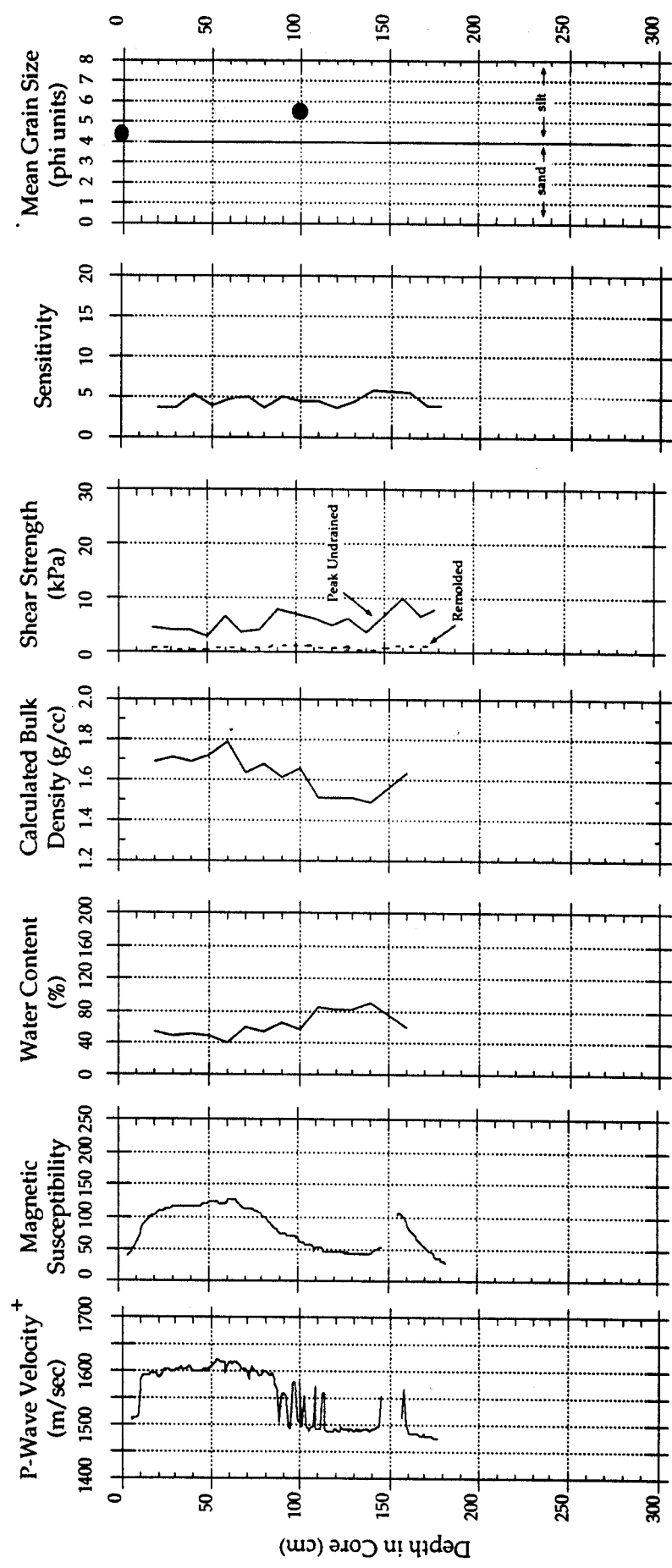
+ Calibration Incomplete

Preliminary Data: Not for Release or Publication

Cruise ID: F8-90-NC
Core: 6G7

FARALLON SLOPE STUDY

Transect B
Water Depth: 795 m
Environment: Upper Slope



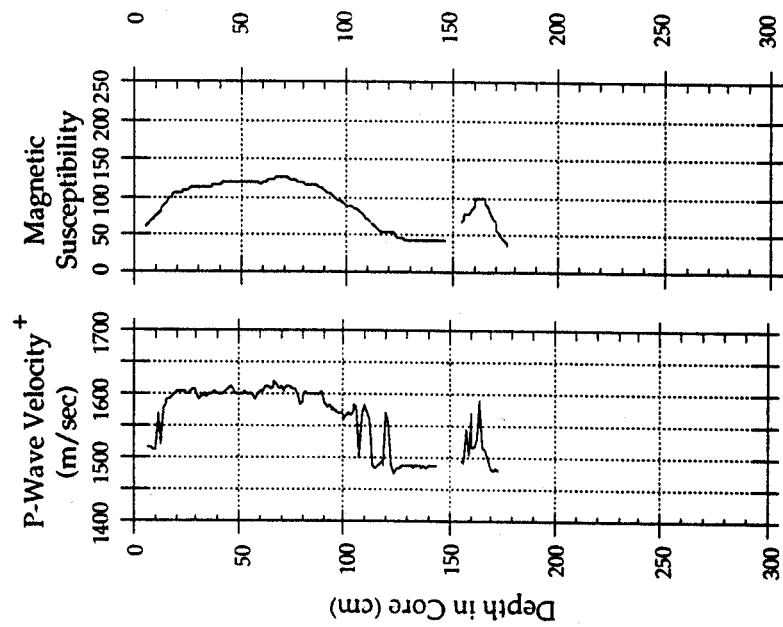
+ Calibration Incomplete

Preliminary Data: Not for Release or Publication

Cruise ID: F8-90-NC
Core: 6G8

FARALLON SLOPE STUDY

Transsect B
Water Depth: 800 m
Environment: Upper Slope



+ Calibration Incomplete

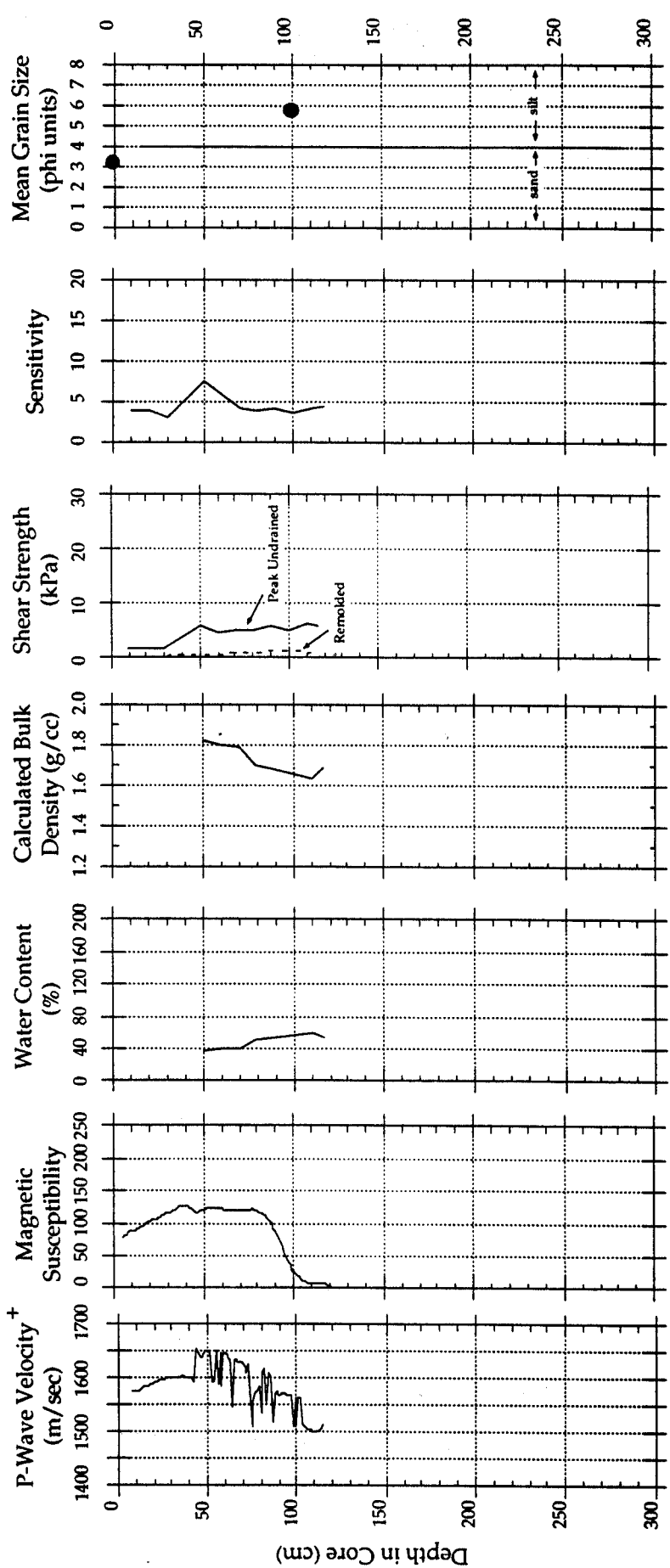
Preliminary Data: Not for Release or Publication

Cruise ID: F8-90-NC

Core: 7G9

FARALLON SLOPE STUDY

Transect B
Water Depth: 716 m
Environment: Upper Slope



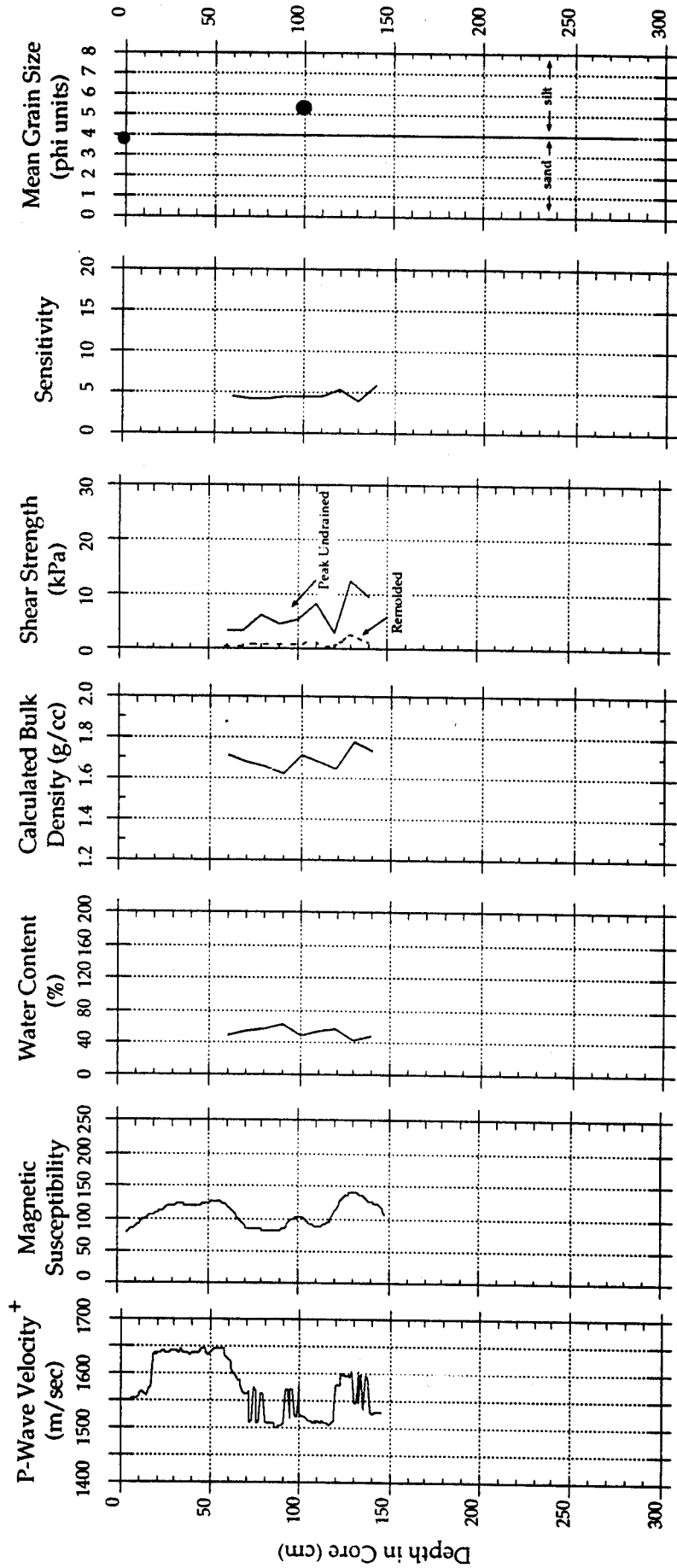
+ Calibration Incomplete

Preliminary Data: Not for Release or Publication

Cruise ID: F8-90-NC
Core: 8G10

FARALLON SLOPE STUDY

Transect B
Water Depth: 537 m
Environment: Upper Slope



+ Calibration Incomplete

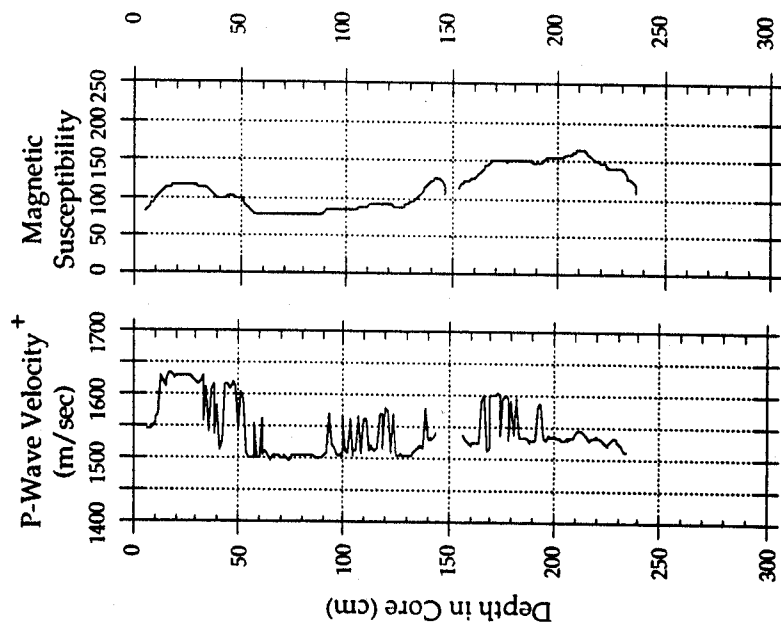
Preliminary Data: Not for Release or Publication

Cruise ID: F8-90-NC

Core: 8G11

FARALLON SLOPE STUDY

Transect B
Water Depth: 540 m
Environment: Upper Slope



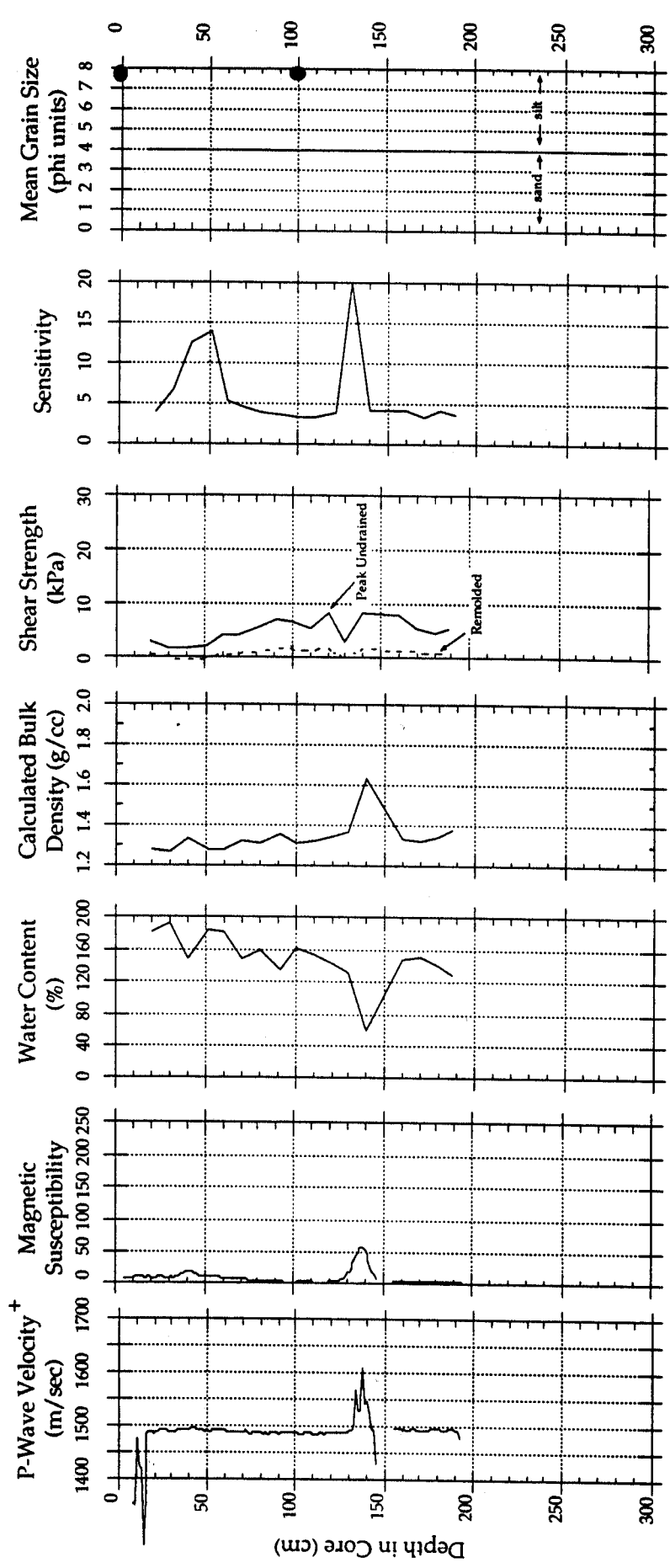
+ Calibration Incomplete

Preliminary Data: Not for Release or Publication

Cruise ID: F8-90-NC
Core: 11G12

FARALLON SLOPE STUDY

Transect C
Water Depth: 3120 m
Environment: Base-of-Slope



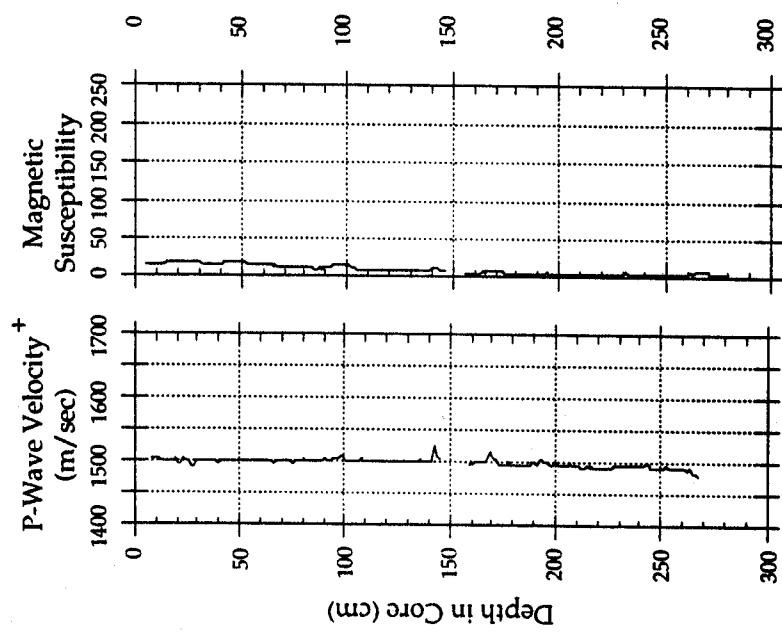
+ Calibration Incomplete

Preliminary Data: Not for Release or Publication

Cruise ID: F890-NC
Core: 12G14

FARALLON SLOPE STUDY

Transect B
Water Depth: 2710 m
Environment: Base-of-Slope



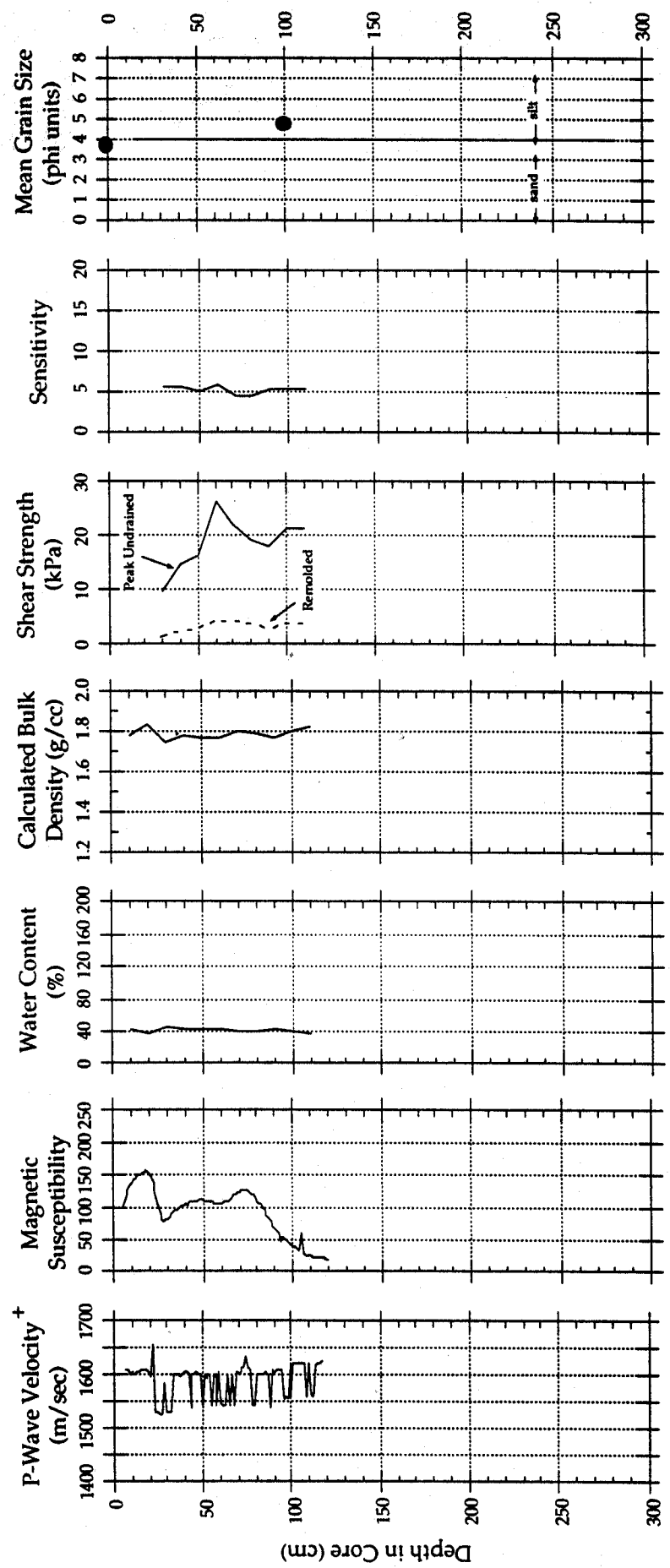
+ Calibration Incomplete

Preliminary Data: Not for Release or Publication

Cruise ID: F890-NC
Core: 16G17

FARALLON SLOPE STUDY

Transect C
Water Depth: 280 m
Environment: Upper Slope



+ Calibration Incomplete

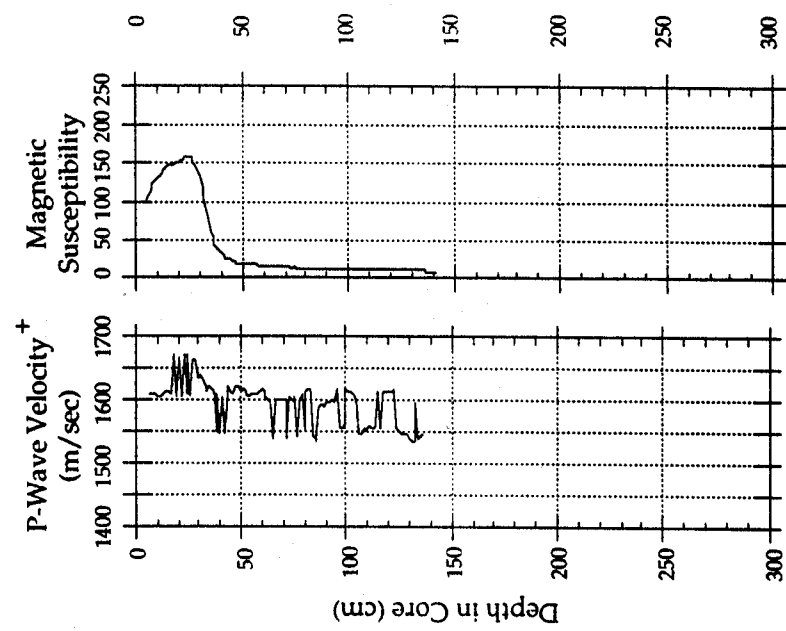
Preliminary Data: Not for Release or Publication

Cruise ID: F8-90-NC

Core: 16G18

FARALLON SLOPE STUDY

Transect C
Water Depth: 276 m
Environment: Upper Slope



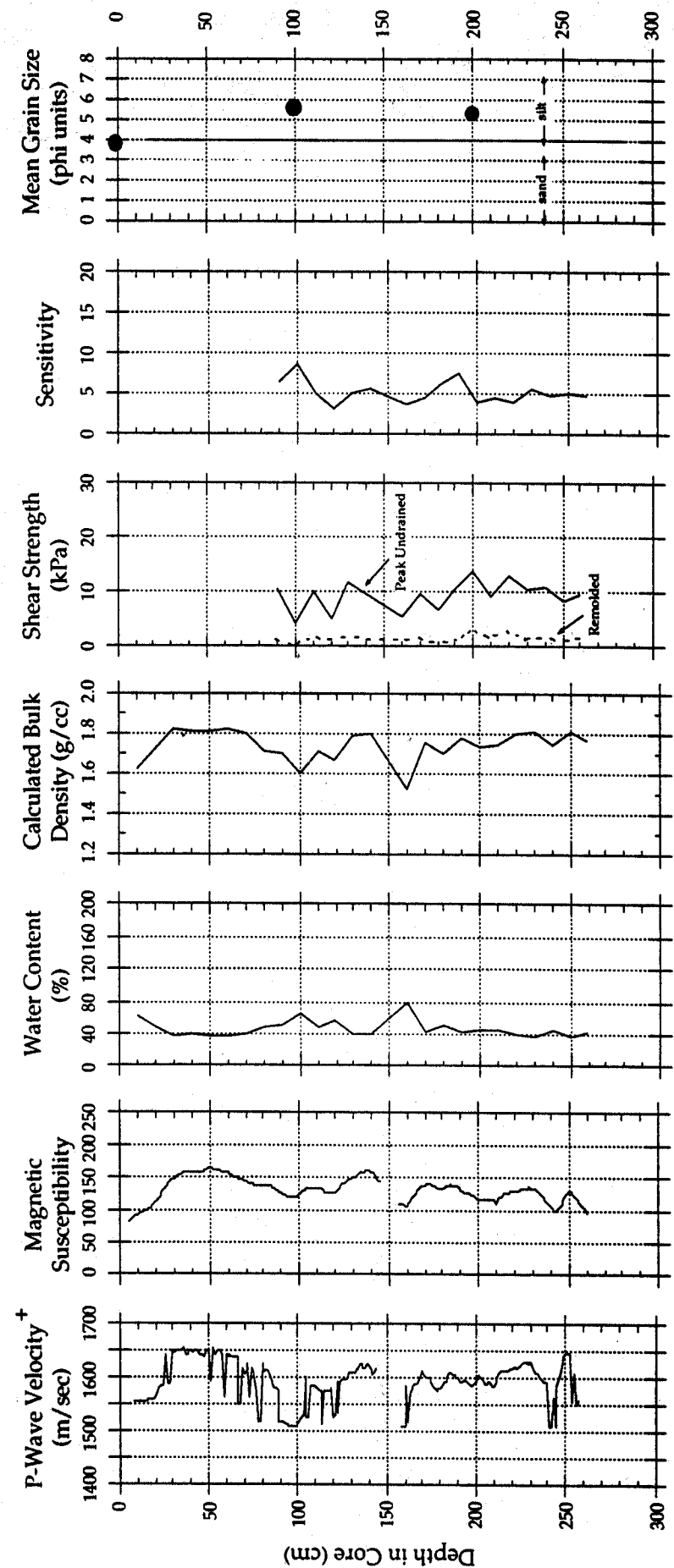
+ Calibration Incomplete

Preliminary Data: Not for Release or Publication

Cruise ID: F8-90-NC
Core: 17G19

FARALLON SLOPE STUDY

Transect C
Water Depth: 670 m
Environment: Upper Slope



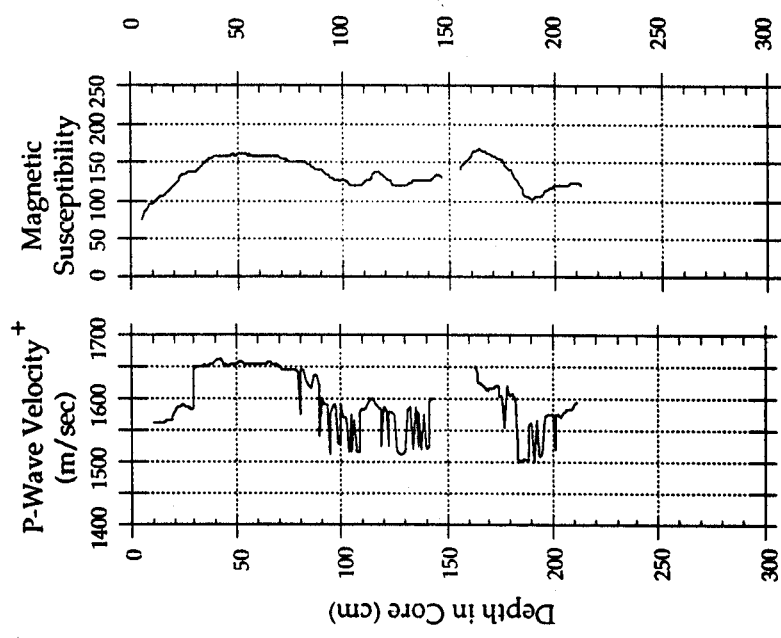
+ Calibration Incomplete

Preliminary Data: Not for Release or Publication

Cruise ID: F8-90-NC
Core: 17G20

FARALLON SLOPE STUDY

Transect C
Water Depth: 665 m
Environment: Upper Slope



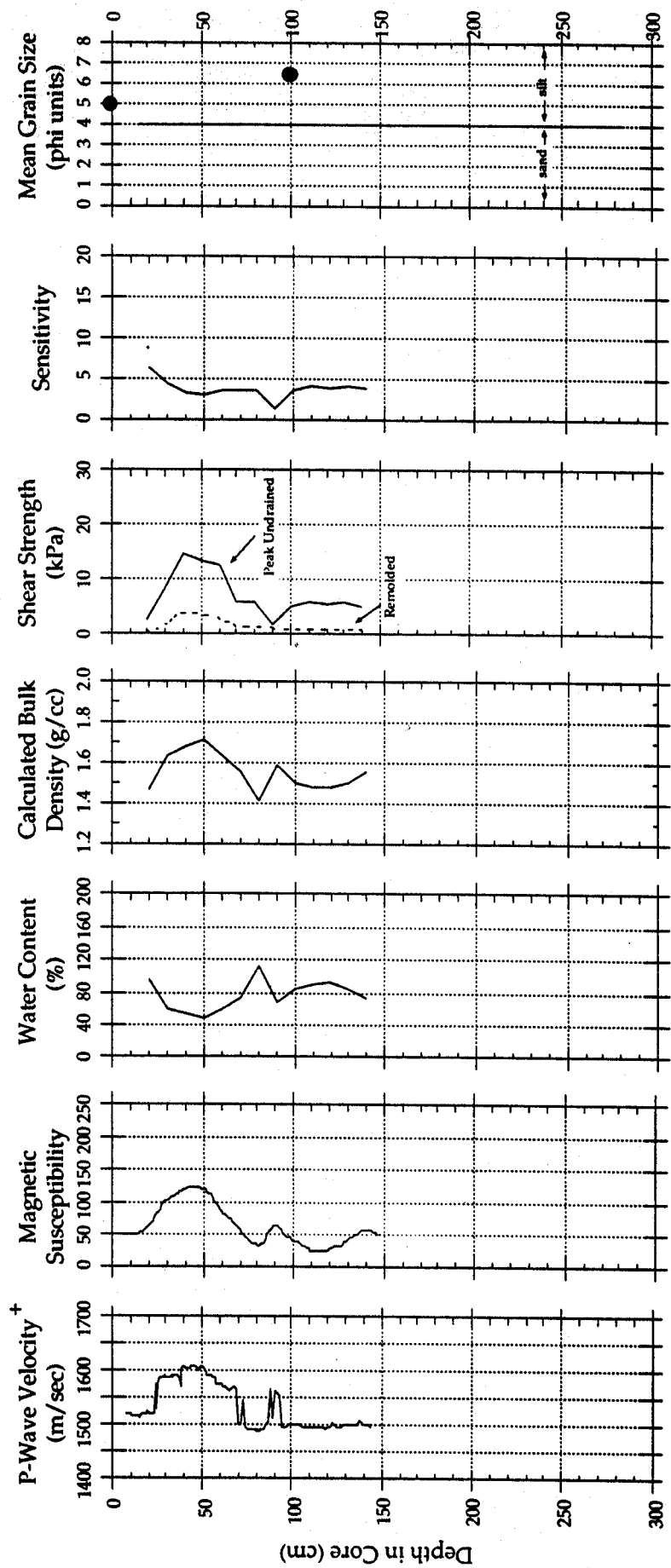
+ Calibration Incomplete

Preliminary Data: Not for Release or Publication

Cruise ID: F8-90-NC
Core: 18G21

FARALLON SLOPE STUDY

Transect C
Water Depth: 1605 m
Environment: Lower Slope



+ Calibration Incomplete

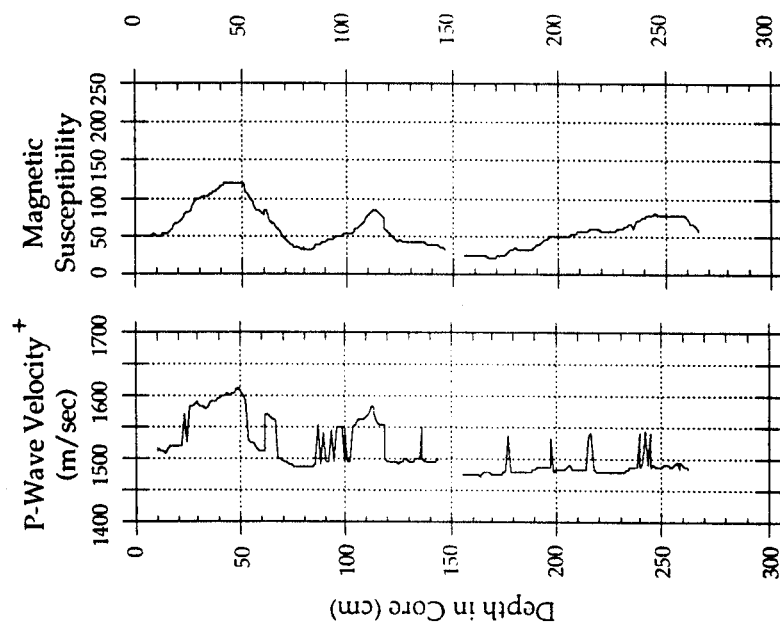
Preliminary Data: Not for Release or Publication

Cruise ID: F8-90-NC

Core: 18G22

FARALLON SLOPE STUDY

Transect C
Water Depth: 1604 m
Environment: Lower Slope



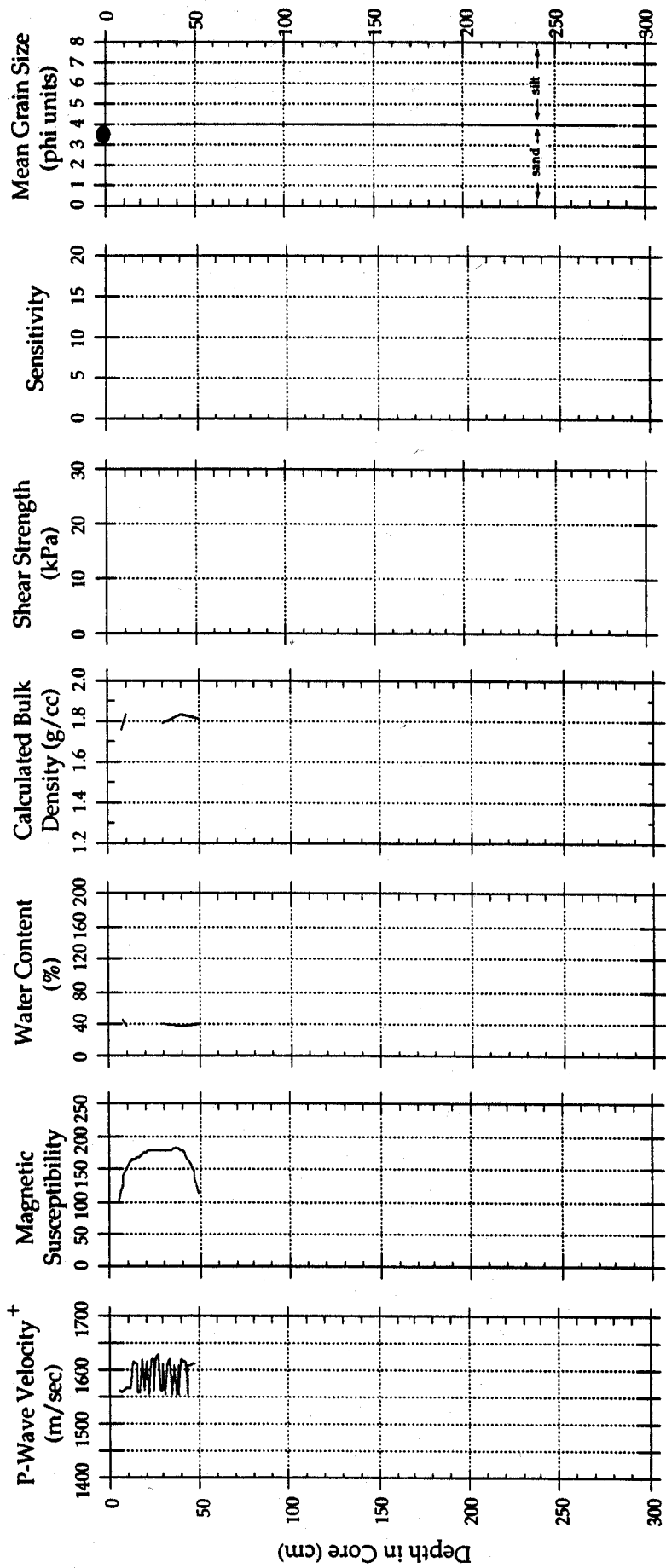
+ Calibration Incomplete

Preliminary Data: Not for Release or Publication

Cruise ID: F8-90-NC
Core: 19G23

FARALLON SLOPE STUDY

Water Depth: 630 m
Environment: Upper Slope



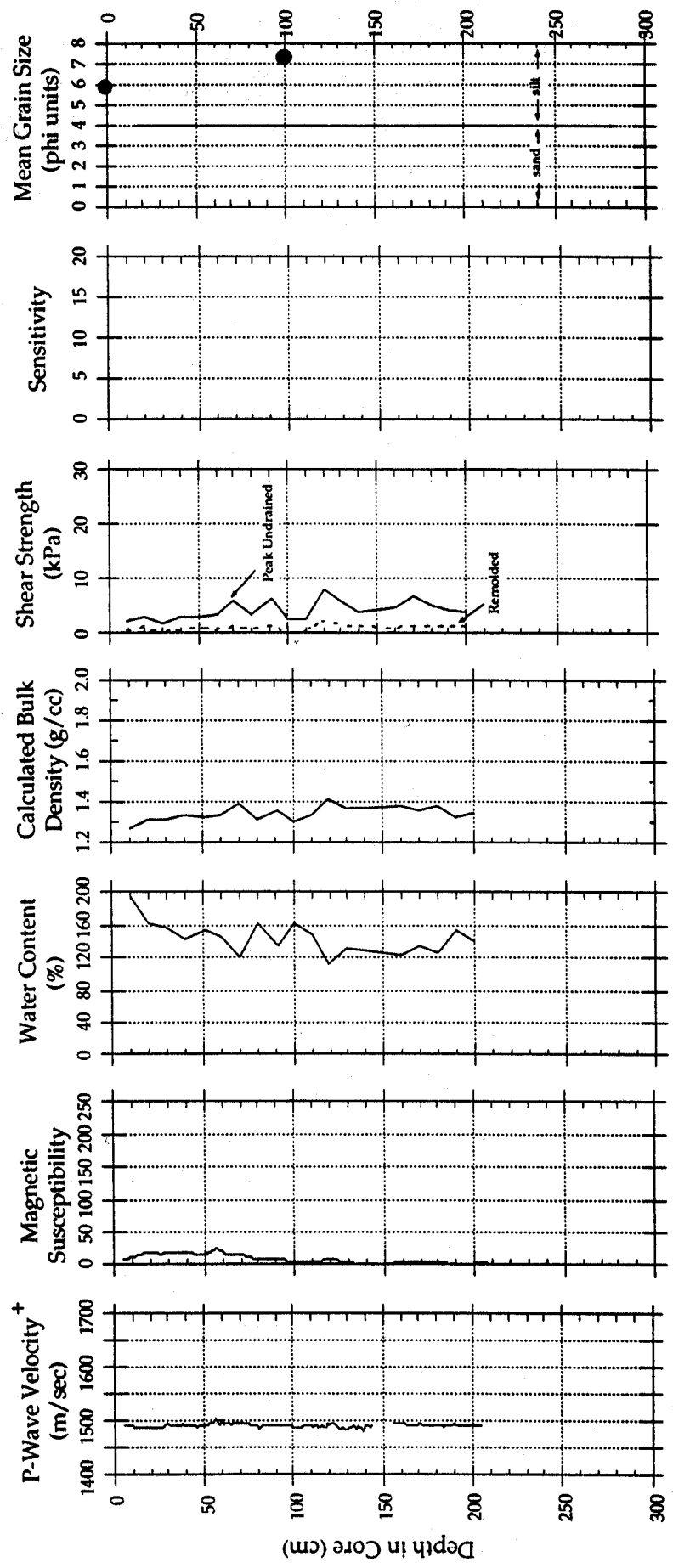
+ Calibration Incomplete

Preliminary Data: Not for Release or Publication

Cruise ID: F890-NC
Core: 20G24

FARALLON SLOPE STUDY

Transect A
Water Depth: 2495 m
Environment: Base-of-Slope



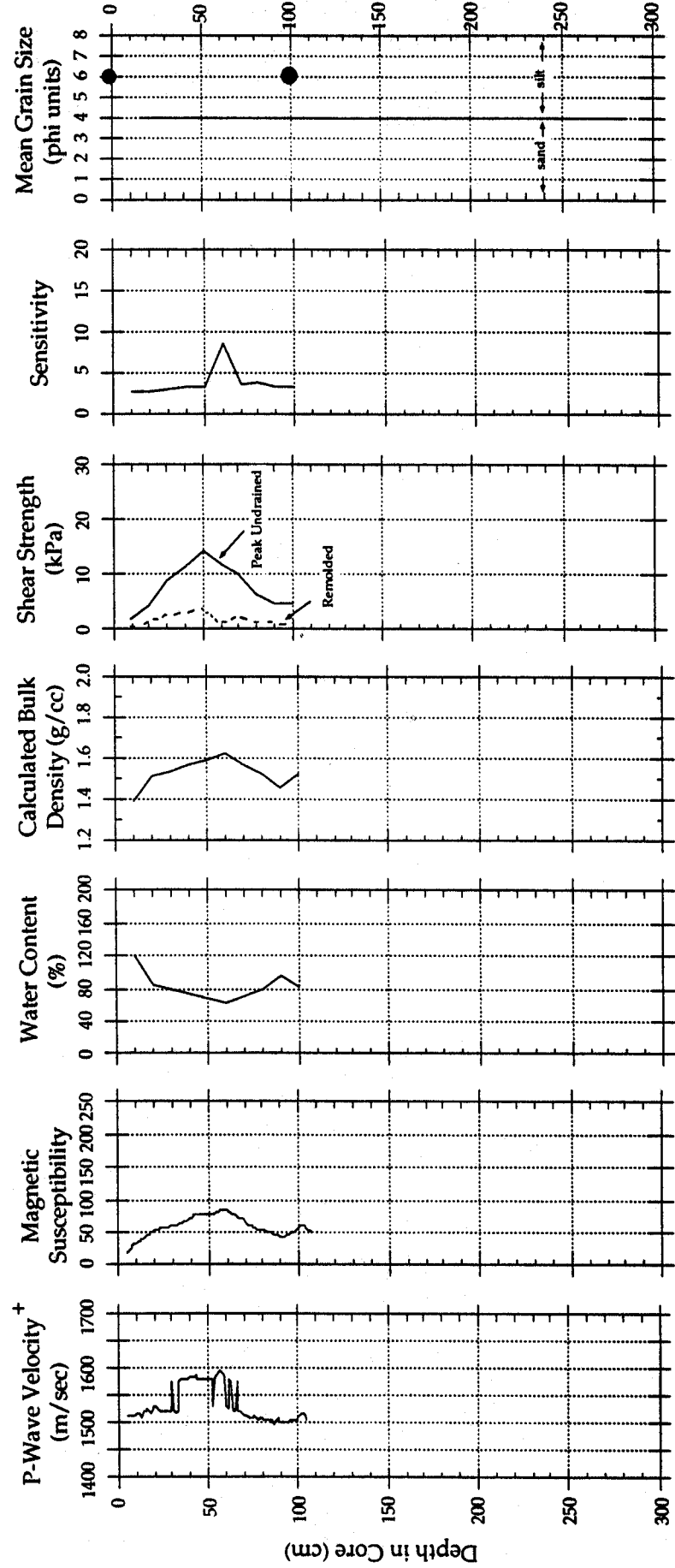
+ Calibration Incomplete

Preliminary Data: Not for Release or Publication

Cruise ID: F8-90-NC
Core: 21G25

FARALLON SLOPE STUDY

Transect A
Water Depth: 1720 m
Environment: Lower Slope



⁺ Calibration Incomplete

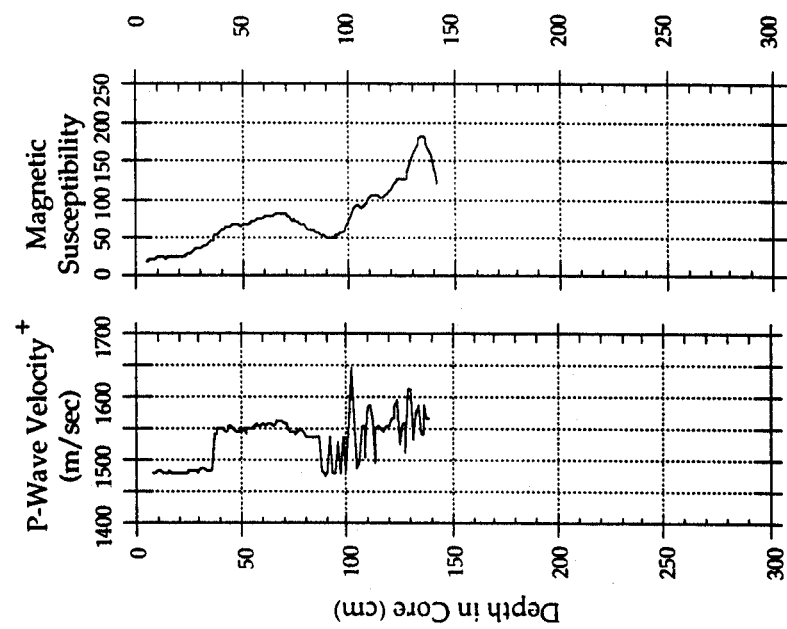
Preliminary Data: Not for Release or Publication

Cruise ID: F8-90-NC

Core: 21G26

FARALLON SLOPE STUDY

Transect A
Water Depth: 1720 m
Environment: Lower Slope



+ Calibration Incomplete

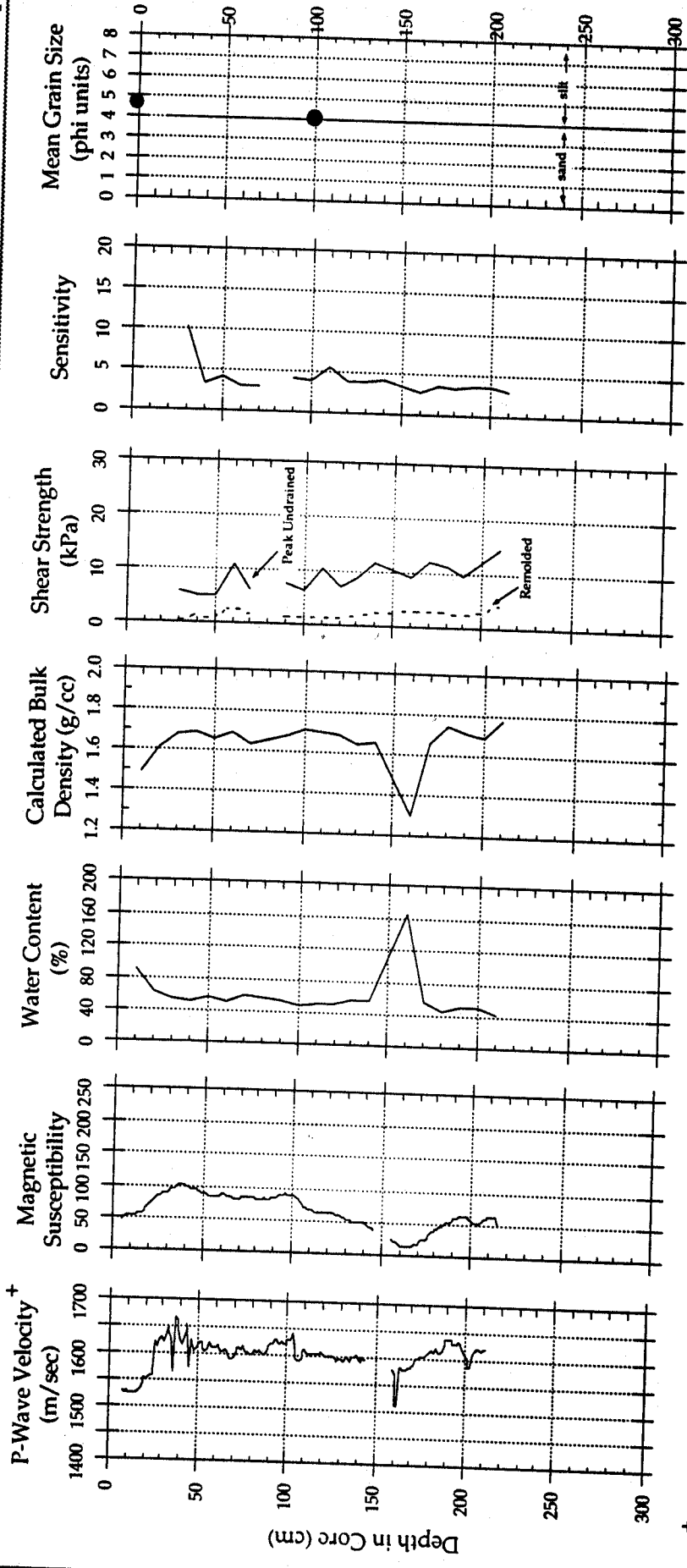
Preliminary Data: Not for Release or Publication

Cruise ID: F8-90-NC

Core: 23G27

FARALLON SLOPE STUDY

Transect A
Water Depth: 1378 m
Environment: Middle Slope



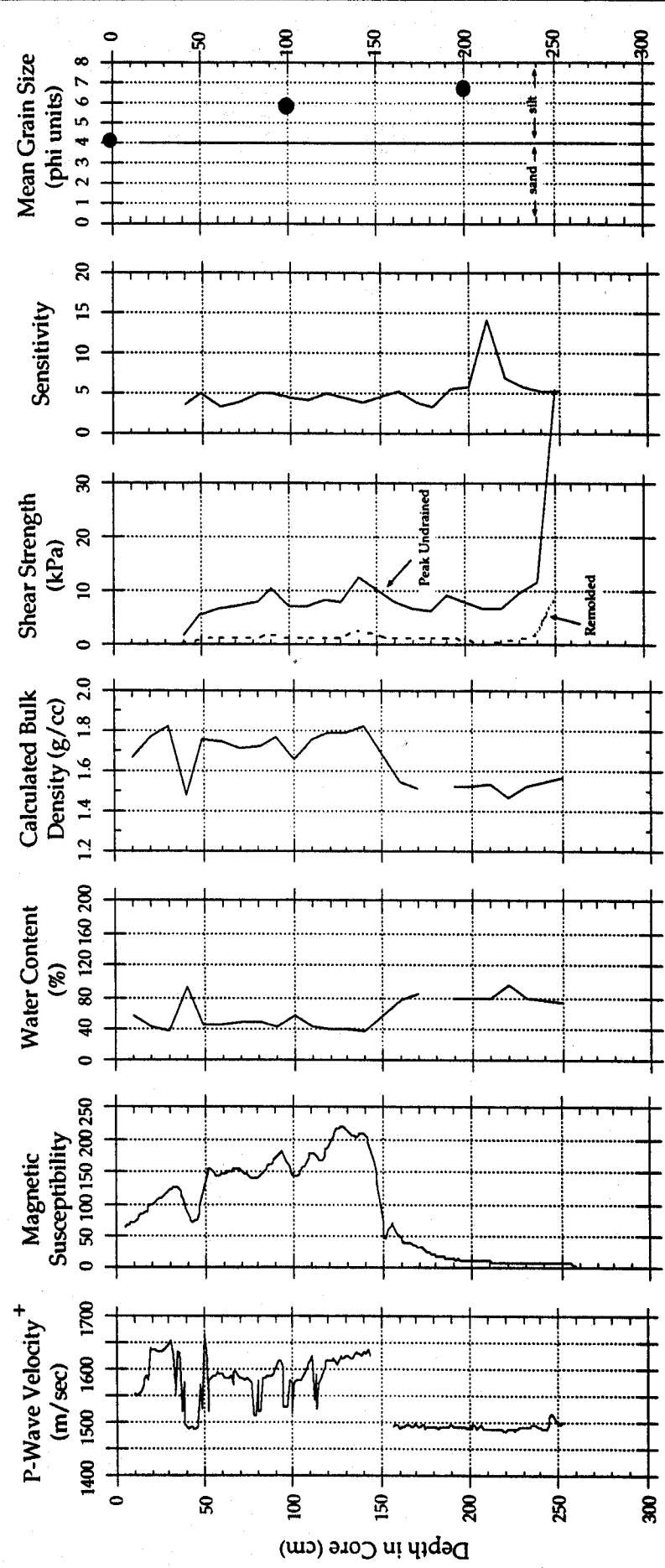
+ Calibration Incomplete

Preliminary Data: Not for Release or Publication

Cruise ID: F8-90-NC
Core: 24G28

FARALLON SLOPE STUDY

Transect A
Water Depth: 970 m
Environment: Middle Slope



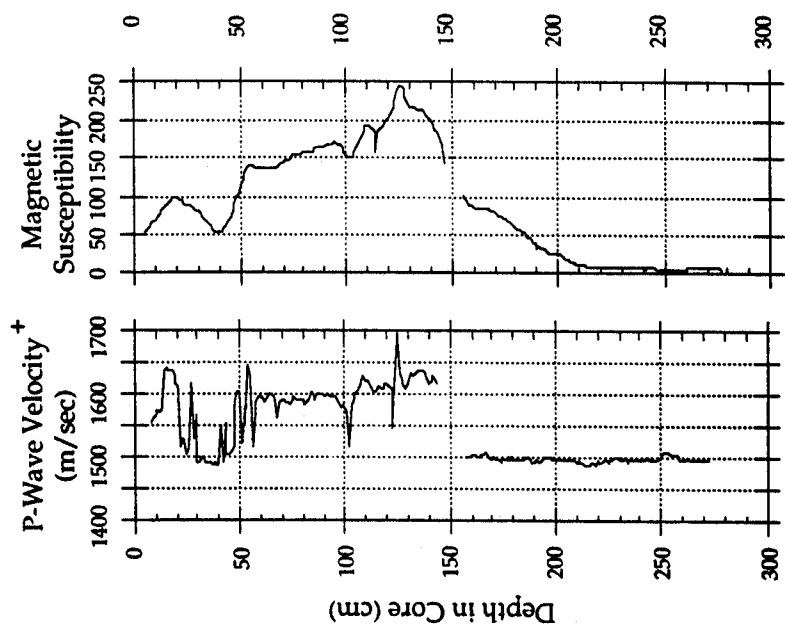
+ Calibration Incomplete

Preliminary Data: Not for Release or Publication

Cruise ID: F8-90-NC
Core: 24G29

FARALLON SLOPE STUDY

Transect A
Water Depth: 970 m
Environment: Middle Slope



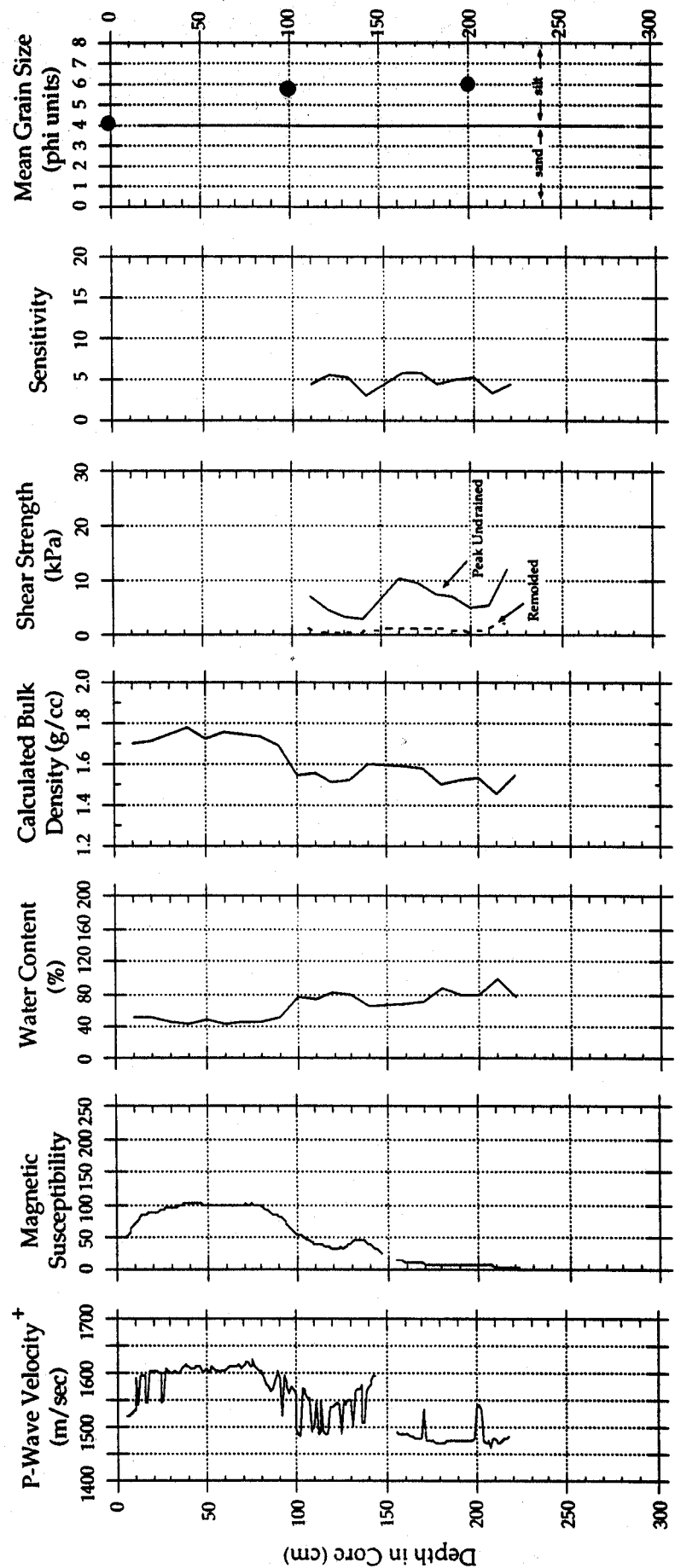
+ Calibration Incomplete

Preliminary Data: Not for Release or Publication

Cruise ID: F8-90-NC
Core: 26G31

FARALLON SLOPE STUDY

Water Depth: 728 m
Environment: Upper Slope



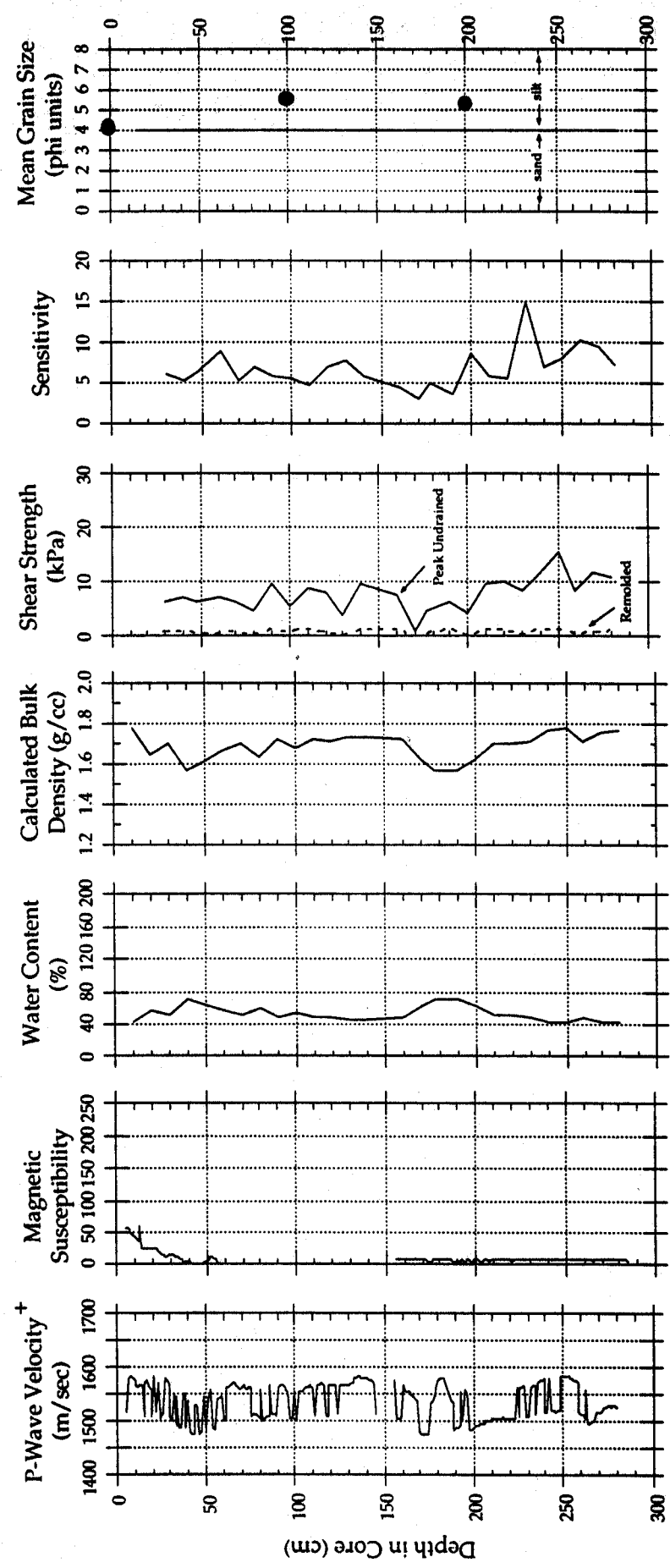
+ Calibration Incomplete

Preliminary Data: Not for Release or Publication

Cruise ID: F890-NC
Core: 27G32

FARALLON SLOPE STUDY

Transect C
Water Depth: 638 m
Environment: Upper Slope



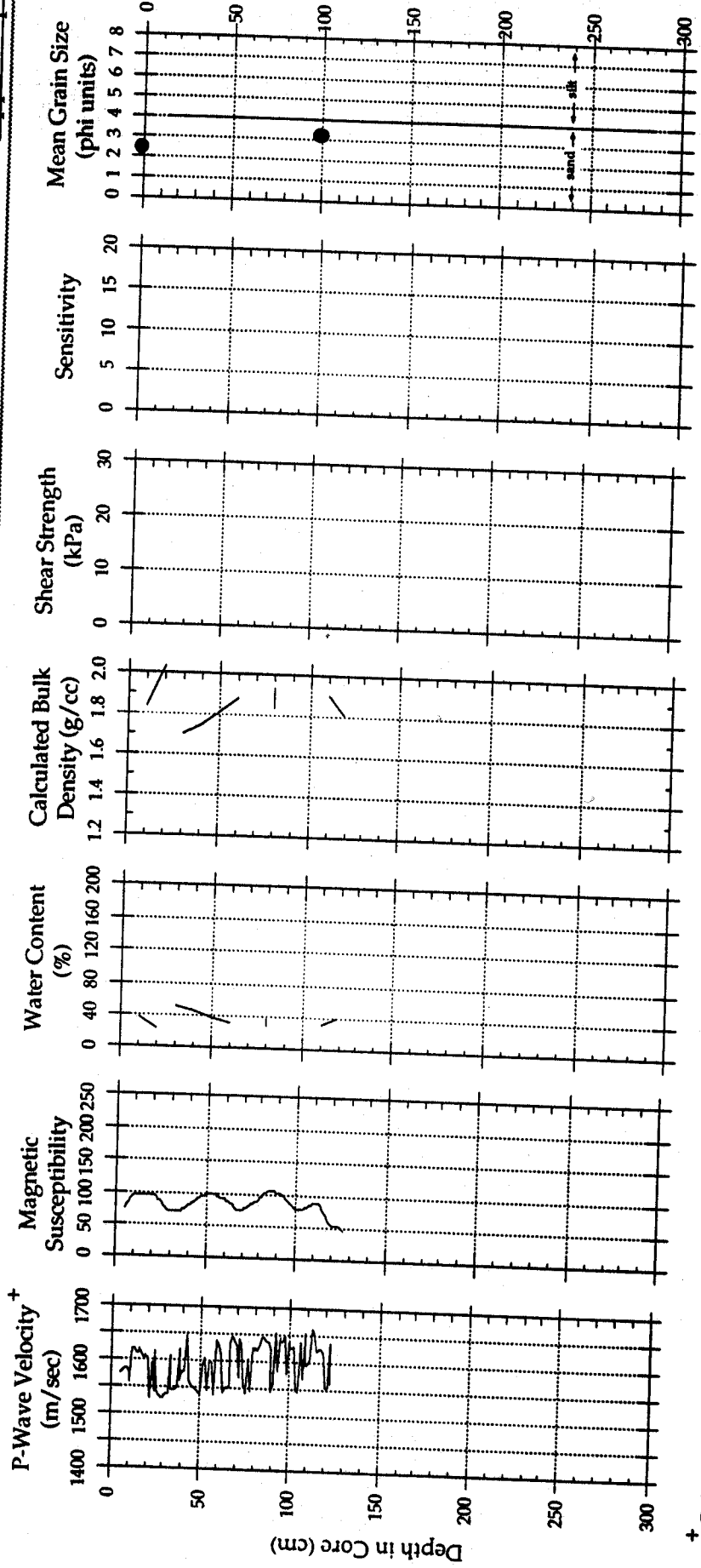
+ Calibration Incomplete

Preliminary Data: Not for Release or Publication

Cruise ID: F8-90-NC
Core: 29G34

FARALLON SLOPE STUDY

Transect C
Water Depth: 685 m
Environment: Upper Slope



+ Calibration Incomplete

Preliminary Data: Not for Release or Publication